



## OPEN ACCESS

## EDITED BY

Steven L. Forman,  
Baylor University, United States

## REVIEWED BY

Gabor Ujvari,  
Hungarian Academy of Sciences (MTA),  
Hungary  
Nadia Solovieva,  
University College London,  
United Kingdom

## \*CORRESPONDENCE

Ozan Mert Göktürk,  
✉ ozan.gokturk@uib.no  
Margit H. Simon,  
✉ msim@norceresearch.no

†These authors have contributed equally to this work and share first authorship

RECEIVED 31 March 2023

ACCEPTED 16 June 2023

PUBLISHED 25 July 2023

## CITATION

Göktürk OM, Simon MH, Sobolowski SP, Zhang Z, Van Der Bilt W, Mørkved PT, D'Andrea WJ, van Niekerk KL, Henshilwood CS, Armitage SJ and Jansen E (2023), Behaviourally modern humans in coastal southern Africa experienced an increasingly continental climate during the transition from Marine Isotope Stage 5 to 4. *Front. Earth Sci.* 11:1198068. doi: 10.3389/feart.2023.1198068

## COPYRIGHT

© 2023 Göktürk, Simon, Sobolowski, Zhang, Van Der Bilt, Mørkved, D'Andrea, van Niekerk, Henshilwood, Armitage and Jansen. This is an open-access article distributed under the terms of the [Creative Commons Attribution License \(CC BY\)](https://creativecommons.org/licenses/by/4.0/). The use, distribution or reproduction in other forums is permitted, provided the original author(s) and the copyright owner(s) are credited and that the original publication in this journal is cited, in accordance with accepted academic practice. No use, distribution or reproduction is permitted which does not comply with these terms.

# Behaviourally modern humans in coastal southern Africa experienced an increasingly continental climate during the transition from Marine Isotope Stage 5 to 4

Ozan Mert Göktürk<sup>1,2\*†</sup>, Margit H. Simon<sup>1,3,4\*†</sup>, Stefan Pieter Sobolowski<sup>1,3</sup>, Zhongshi Zhang<sup>1,3</sup>, Willem Van Der Bilt<sup>2</sup>, Pål Tore Mørkved<sup>2</sup>, William J. D'Andrea<sup>4</sup>, Karen L. van Niekerk<sup>1,5</sup>, Christopher S. Henshilwood<sup>1,6</sup>, Simon J. Armitage<sup>1,7</sup> and Eystein Jansen<sup>1,2,3</sup>

<sup>1</sup>SFF Centre for Early Sapiens Behaviour (SapienCE), University of Bergen, Bergen, Norway, <sup>2</sup>Department of Earth Science, University of Bergen, Bjercknes Centre for Climate Research, Bergen, Norway, <sup>3</sup>NORCE Norwegian Research Centre, Bjercknes Centre for Climate Research, Bergen, Norway, <sup>4</sup>Lamont-Doherty Earth Observatory, Columbia University, Palisades, NY, United States, <sup>5</sup>School of Geography, Archaeology and Environmental Studies, University of Witwatersrand, Johannesburg, South Africa, <sup>6</sup>Evolutionary Studies Institute, University of the Witwatersrand, Johannesburg, South Africa, <sup>7</sup>Department of Geography, Royal Holloway University of London, Surrey, United Kingdom

Linking human technological and behavioural advances to environmental changes is challenging, as it requires a robust understanding of past climate at local scales. Here, we present results from regional high-resolution numerical simulations along with climate data directly from the archaeological sequence of Blombos Cave (BBC), a well-studied site in coastal southern Africa. The model simulations cover two distinct periods centred at 82 and 70 thousand years (ka) ago (Marine Isotope Stage [MIS] 5 and the onset of MIS 4, respectively), when orbital parameters and global sea level were markedly different from one another. Climatic changes from 82 to 70 ka are determined through four simulations that use past and present-day coastline configurations. The hydrogen isotopic composition of leaf waxes ( $\delta^2\text{H}_{\text{wax}}$ ) and *n*-alkane distributions and abundances are used to reconstruct hydroclimate around BBC. The leaf wax *n*-alkane record, one of the first produced in an archaeological setting in this region to date, can be interpreted as a drying signal from MIS 5c to 4. This agrees with our modelling results, which indicate a drier and more continental climate over coastal southern Africa at 70 ka, compared to 82 ka. The simulated aridification is most evident from the reduced precipitation amounts in both summer (~20%) and winter (~30%). The annual number of summer days ( $T_{\text{max}} \geq 25^\circ\text{C}$ ) and cold nights ( $T_{\text{min}} < 5^\circ\text{C}$ ) in the vicinity of BBC increases more than 5 and 3-fold, respectively, under the more continental climate at 70 ka. Weaker westerly winds in winter, a cooler Agulhas Current, and a land surface expansion associated with the coastline shift due to lower sea levels at 70 ka all contribute to the simulated climate shift. Our approach highlights the importance of multiple lines of evidence for achieving robust results, while demonstrating how both large-scale forcing and local influences worked together in shaping the local climate that early humans lived in. Adaptation to a

drier climate and increased continentality around BBC might have induced greater mobility, which led to increased population interactions, cultural transmission rates, skill exchange, and material complexity during the so-called Still Bay period.

#### KEYWORDS

southern Africa, palaeoclimate, regional modelling, proxy, leaf wax n-alkanes, middle stone age, modern human behaviour

## 1 Introduction

Southern Africa hosted major phases of cultural, technological, and subsistence innovation by early *Homo sapiens* (*H.sapiens*), notably the Still Bay and Howiesons Poort technological complexes, dated to  $76.0 \pm (3.3, 5.6)$  ka -  $71.0 \pm (3.8, 5.7)$  ka, and  $65.5 \pm 4.8$  ka to  $59.4 \pm 4.6$  ka, respectively (Henshilwood et al., 2014; Jacobs et al., 2020). These time periods are positioned within major global and regional climate shifts associated with Marine Isotope Stage (MIS) 5 (ca. 128–71 ka) to 4 (ca. 70–60 ka), (Singarayer and Burrough, 2015; Carr et al., 2016). The cultural adaptation that occurred in these two phases, which was both of technological and symbolic nature, appears in the archaeological record as coherent and recognizable evidence and has an intricacy comparable to the innovations seen in modern hunter-gatherers (d’Errico et al., 2017). The Still Bay is a Middle Stone Age (MSA) stone tool manufacturing style during which people produced heat-treated, pressure-flaked technologies (Mourre et al., 2010). The Howiesons Poort is distinguished by complex hafting technologies and hunting strategies (Lombard, 2011). It has been argued that the innovations found during both of these periods were already emerging during the earlier MIS 5 pre-Still Bay period, although not all the benefits had been realized yet (Porráz et al., 2021).

More specifically, South Africa has yielded some of the best-preserved continuous stratigraphic evidence for human behavioural evolution, with sites such as Blombos Cave (BBC) (100–72 ka),

Klipdrift Shelter (66–59 ka), and the MSA deposits at Klasies River, Diepkloof Rock Shelter and Pinnacle Point 13B (Figure 1) (Wurz, 2002; Marean et al., 2007; Henshilwood, 2012; Texier et al., 2013; Henshilwood et al., 2014; Henshilwood et al., 2018; Will et al., 2019). Archaeological findings indicate that during the period 100–50 ka *H. sapiens* populations in South Africa started to exhibit behaviour typically associated with historical hunter-gatherers (i.e., modern humans), such as the use of predominantly red pigment and body ornaments, the production of specialised tools, and the creation of abstract symbolic material culture (d’Errico and Henshilwood, 2007; Henshilwood et al., 2002; Henshilwood et al., 2011; Henshilwood et al., 2018; Soriano et al., 2015).

Despite the wealth of finds at South African sites, we do not fully understand how and why these technological and symbolic innovations evolved, the exact use or meaning of some of these, and why some of these innovations subsequently disappear from the archaeological record. One step towards understanding this is to investigate the potential role that regional and local climate and other environmental variability played in shaping the behaviours of early modern humans. For instance, previous research has mainly focused on the impact of the Palaeo-Agulhas plain on the lives of early humans as a foraging landscape (Haaland et al., 2020; Marean et al., 2020), as the sea level fell, and the land area expanded. However, what would happen to the local climate when the southern African coastline moved seaward exposing a large area of land, has been studied only recently (Göktürk et al., 2023). This

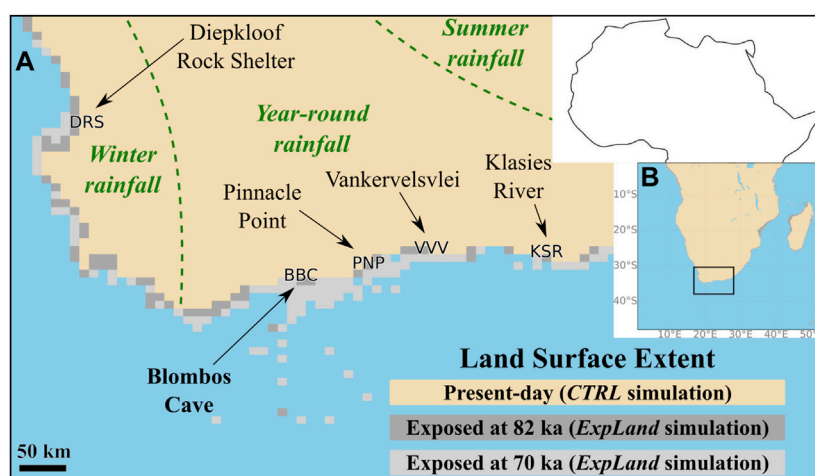


FIGURE 1

(A) Detailed view of the southern Cape and adjacent regions (small black rectangle in b)), along with the locations of Blombos Cave (BBC), Diepkloof Rock Shelter (DRS), Pinnacle Point (PNP), Vankervelsvlei (VVV) and Klasies River Cave (KSR) referred to in the text. Present-day, 70 ka and 82 ka land extents used in the regional climate model are also shown. (B) Regional climate model (WRF) simulation domain (colored part of the figure). Small black rectangle shows the map extent of part (A).

was done through a regional climate model experiment at a single epoch (70 ka) in order to estimate the climate sensitivity of the region to changes in land extent only, keeping the rest of the model configuration unchanged. Whether or how sea level fluctuations, and the accompanying coastline shift, modulated large-scale climate changes at local to regional spatial scales through time, are yet to be explored. Therefore, a logical continuation of the aforementioned work is to extend these analyses into two epochs.

In the current study, we build upon and go beyond Göktürk et al. (2023), by focusing on the differences between MIS 5a at 82 ka and the onset of the glacial MIS 4 at 70 ka. We consider changes arising from the significant shift in orbital forcing, the cooling of sea surface temperatures (Supplementary Figure S1), and the regression of the coastline due to a ~40 m decrease in global sea level from 82 to 70 ka (Grant et al., 2012) (Figure 1). We use climate simulations over southern Africa at these two epochs, performed with a high-resolution regional climate model (RCM) driven by a coupled, IPCC-class general circulation model (GCM). The simulation results at 70 ka, which were used to investigate the effects of an idealized coastline shift (Göktürk et al., 2023), are extended in this study with the addition of new simulations at 82 ka. We then compare the output of these high-resolution climate simulations with climatic observations from a new (~90–68 ka) record of  $\delta^2\text{H}$  and *n*-alkane distributions and abundances, measured on leaf waxes from the archaeological sequence of BBC. Plant wax biomarkers have not been widely utilized by archaeologists and paleoanthropologists yet, although they serve as a traditional tool in Earth sciences, especially in climate studies based on ocean and lake sediment records. Our leaf wax *n*-alkane-based palaeoenvironmental reconstruction reflects changes in vegetation and hydroclimate, allowing us to derive key climate information directly from within the archaeological layers of the site. Lastly, we place our environmental findings into the context of known evidence from archaeological sites in the Southern Cape, South Africa and the development of modern human behaviour among *H. sapiens* at that time.

## 2 Study area: Blombos Cave background and regional setting

Blombos Cave (BBC) is situated on the southern coast of South Africa approximately 300 km east of Cape Town within a private Nature Reserve (Figure 1A). Today the cave is 34.5 m above modern sea level in a south-facing calcarenite cliff (Haaland et al., 2020). The present-day shoreline is approximately 80 m away from the cave location (Figure 1).

BBC is one of the best-dated archaeological sites in South Africa. The chronology for the cave's sediment sequence is based on detailed optically stimulated luminescence (OSL) dating (Jacobs et al., 2020). The sequence spans from  $108 \pm 12.1$  ka at the base of the current excavation to  $71.0 \pm 5.7$  ka at the top (Jacobs et al., 2020) (all age uncertainties are reported at 95.4% confidence interval hereafter, using the second uncertainty reported by Jacobs et al., 2020, which is the total uncertainty including shared errors). The MSA levels of BBC are divided into three phases: M1 (layers CD-CA), M2 upper (layers CFD-CF), M2 lower (layers GCAC-CGAA), and M3 (layers CPA-CH)

(Figure 2). The M1 and upper M2 phases contain the Still Bay technological complex and are dated to ~76.0–71.0 ka (MIS 5a). The M3 layers were deposited between about 100 and 90 ka (MIS 5c to 5b). A culturally sterile layer of undisturbed sand (DUN) overlies the MSA sequence (start of MIS 4) and was apparently emplaced  $\sim 71 \pm 5.7$  ka when a near-continuous sand body covered the Blombos coast and buried the entrance to BBC (Jacobs et al., 2020).

South Africa is characterised by three major seasonal rainfall zones in the present day (Figure 1). The Summer Rainfall Zone (SRZ) covers the eastern and central parts of the country, where the majority (>66%) of rainfall is sourced from the tropics and falls during the austral summer (Nicholson, 2000). The Winter Rainfall Zone (WRZ), where most (>66%) of the rainfall is brought by midlatitude storms during austral winter, covers a narrow belt along the west coast (Nicholson, 2000). An intermediate area between the SRZ and WRZ receives rainfall from both sources throughout the year (Year-round Rainfall Zone (YRZ)) (Nicholson, 2000). The YRZ includes the southern Cape coast, where BBC is located, and is the region of interest for this investigation. At present the Blombos area experiences annual rainfall of ~500–600 mm (Nel and Henshilwood, 2016) with approximately 56% of this amount being received during the winter half of the year (Fick and Hijmans, 2017). The rainfall in the YRZ is driven by interactions between tropical, subtropical, and temperate weather systems (Engelbrecht and Landman, 2016). Moreover, anticyclonic circulation produces onshore flow that leads to orographic rainfall from local sources (Weldon and Reason, 2014; Engelbrecht and Landman, 2016). The isotopic changes in the precipitation are related to both large-scale transport by synoptic weather systems and locally-derived moisture sources that can also be observed in the modern day at seasonal and interannual timescales (Engelbrecht and Landman, 2016). Measurements of seasonal and yearly  $\delta^2\text{H}$  values from the YRZ show that precipitation isotopes vary with the occurrence of the main synoptic types such as tropical - temperate troughs (Braun et al., 2017).

Three main biomes characterise the region around BBC today are: fynbos (~90%), succulent Karoo (~9%) and Albany thicket (~1%) (Mucina and Rutherford, 2006), with fynbos and thicket dominating the immediate vicinity of the cave (Nel and Henshilwood, 2016).

## 3 Materials and methods

In this study, we aim to investigate local to regional climate characteristics during periods of human occupation on the South African coastline within the last glacial cycle. To do this, we compare model simulations and proxy-based reconstructions of climate parameters. Output from a global coupled general circulation model (GCM) was used as forcing data for a regional climate model (RCM) focused on a limited area at much higher resolution. We performed time-slice experiments with the RCM using the present and past coastlines 70 and 82 ka. Concurrently, leaf wax *n*-alkane analyses were performed on archaeological sediments from BBC that provide insight into moisture sources and balance, allowing comparison against the model results.

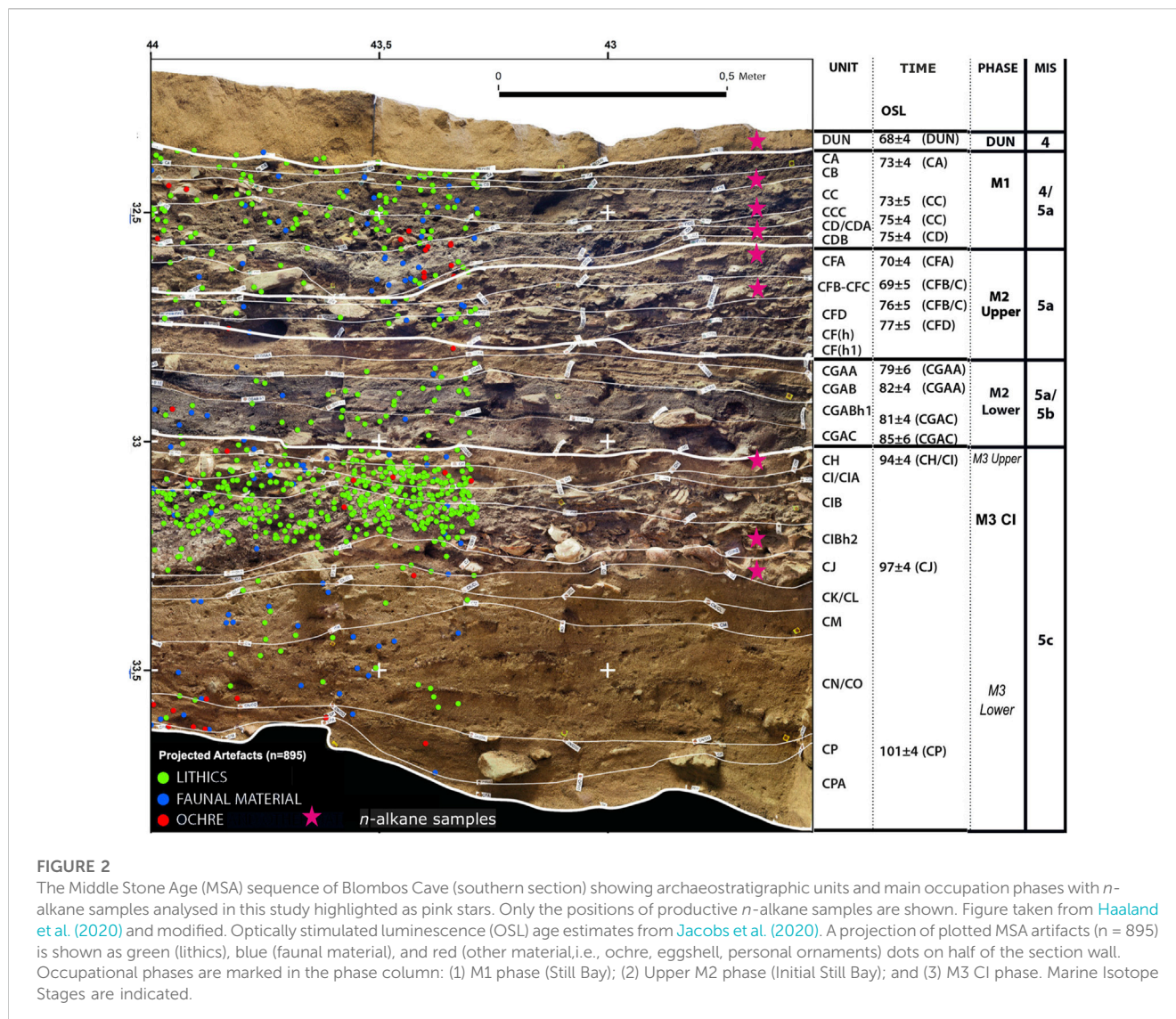


**FIGURE 2**

The Middle Stone Age (MSA) sequence of Blombos Cave (southern section) showing archaeostratigraphic units and main occupation phases with *n*-alkane samples analysed in this study highlighted as pink stars. Only the positions of productive *n*-alkane samples are shown. Figure taken from Haaland et al. (2020) and modified. Optically stimulated luminescence (OSL) age estimates from Jacobs et al. (2020). A projection of plotted MSA artifacts (n = 895) is shown as green (lithics), blue (faunal material), and red (other material, i.e., ochre, eggshell, personal ornaments) dots on half of the section wall. Occupational phases are marked in the phase column: (1) M1 phase (Still Bay); (2) Upper M2 phase (Initial Still Bay); and (3) M3 CI phase. Marine Isotope Stages are indicated.

## 3.1 Climate modelling

We extend the regional climate modelling results already available for 70 ka (Göktürk et al., 2023) by performing new simulations at 82 ka. For additional details regarding the modelling protocol and experiment design, readers are referred to Göktürk et al. (2023).

### 3.1.1 Global model protocol

Global simulations at 70 and 82 ka were conducted using the fast version of the Norwegian Earth System Model (NorESM1-F). A horizontal resolution of  $\sim 2^\circ$  and 26 vertical levels are present in the atmosphere component. The ocean-sea ice component is on a tripolar grid with a nominal  $1^\circ$  resolution and 53 vertical layers in the ocean. Greenhouse gas levels (Martínez-Botí et al., 2015), orbital parameters (Berger and Loutre, 1991), and global mean sea-level (GMSL) drops (Rohling et al., 2014) at 70 and 82 ka can be found in Supplementary Table S1. The changes in the land-sea distribution arising from GMSL variations are also considered in the model setup. For instance at 70 ka, as a result of the 75-m drop of the

GMSL with respect to today, the Bering Strait becomes closed and much of the Sahul, Sunda and East Siberian continental shelves are exposed. The simulations at each epoch were initialised from the Levitus temperature and salinity (Levitus and Boyer, 1994). The model provides output with a temporal resolution of 6 h for the atmosphere, 24 h for land surface, and 1 month for the ocean. The reader is referred to Guo et al. (2019) and Göktürk et al. (2023) for a more detailed description of the global model, including its technical specifications.

### 3.1.2 Regional model protocol

We used the Weather Research and Forecasting Model (WRF) as the RCM. WRF is a limited area atmospheric model that provides geographically detailed information, and is widely used in climate research (Powers et al., 2017). A single domain that covers the entire African continent south of the equator ( $0^\circ$ – $50^\circ$ S,  $0^\circ$ – $55^\circ$ E; Figure 1B) was used to run WRF version 4.5.1 (Skamarock et al., 2019). The horizontal resolution is 12 km, while there are 35 vertical levels between the surface and  $\sim 50$  hPa level. The data generated by the global NorESM1-F simulations (described in the previous

**TABLE 1** Regional climate model (WRF) simulations. The 4 regional climate model (WRF) simulations performed (one per row) and the sea levels used at each simulation. Sea level estimates and associated uncertainties (last 2 columns) are after [Grant et al. \(2012\)](#).

Era	Name of the Simulation	Land Extent	Sea Level (m) wrt Present	Lower Bound of Sea Level (m)	Upper Bound of Sea Level (m)
70 ka	Control ( <i>CTRL</i> )	Present	0	-	-
70 ka	Exposed Land ( <i>ExpLand</i> )	Reconstructed for the era	-80	-90	-70
82 ka	Control ( <i>CTRL</i> )	Present	0	-	-
82 ka	Exposed Land ( <i>ExpLand</i> )	Reconstructed for the era	-42	-52	-30

subsection) were downscaled using WRF, in order to determine climatic changes from 82 ka to 70 ka. There are two 30-year simulations at each epoch, with present-day and reconstructed coastlines (see [Table 1](#) and the next subsection for details). This enables us to disentangle the effects of large scale changes from those of local coastline shifts. Two continuous WRF runs of 10 and 20 years were performed to form one complete downscaling simulation of 30 years. The global model output to be downscaled by WRF was chosen such that the 30-year means of temperature and precipitation at the 20 NorESM grid points around coastal southern Africa have minimal deviation from their long-term averages in the entire NorESM output available. The aim here was to force WRF with boundary conditions that are representative of the NorESM time slice, and to minimize the influence of internal variability. In other words, our model setup helps avoid results being impacted by anomalously warm, cold, wet or dry years, or decades. As model spin-up time an extra year was added to the beginning of each WRF simulation period, to be discarded from the analysis later. Solar radiation calculations within the WRF source code were adjusted using orbital parameters at 82 and 70 ka, as done in [Yoo et al. \(2016\)](#). To obtain high resolution sea surface temperature (SST) input, the *anomaly method* ([Haywood et al., 2010; Zhang and Yan, 2012](#)) was used. This approach makes use of the *anomalies* between the present-day SSTs and the global model's pre-industrial SSTs. The method is superior to using the raw SST output from the global model directly, as it ensures an improved representation of the SSTs in the regional model. The resulting SST input fields for the WRF simulations are on the ERA5 reanalysis ([Hersbach et al., 2020](#)) grid.

### 3.1.3 Coastline changes

To simulate the climatic effects of coastal land extent, the WRF land-sea mask was modified for the exposed land (*ExpLand*) simulations at each epoch ([Figure 1A](#)). This was done by assuming sea levels of -42 and -80 m at 82 and 70 ka, respectively, with respect to present-day sea level, which is used for the control (*CTRL*) simulations. These values, with ranges given in [Table 1](#), are the maximum likelihood estimates in the global mean sea level reconstruction by [Grant et al. \(2012\)](#). This record matches well with the sea level index points determined by [Cawthra et al. \(2018; 2020\)](#) for the southern continental shelf of South Africa. It also has higher temporal resolution and lower age uncertainties compared to other available sea level reconstructions ([Spratt and](#)

[Lisiecki, 2016](#)). On the other hand, we acknowledge that paleo sea level estimates are associated with uncertainties and may not account for local variations in specific regions. For instance, for MIS 5a (~82 ka), [Pico et al. \(2017\)](#) and [Dorale et al. \(2010\)](#) report sea levels that are around present-day values, from the United States mid-Atlantic region and Mallorca, respectively. Yet, we believe the values we use in our regional model are realistic, as sea level for southern Africa tracks global mean sea level estimates, as revealed from the works by [Cawthra et al. \(2018, 2020\)](#) in the area.

## 3.2 Leaf wax *n*-alkane biomarker analysis

### 3.2.1 Materials and lipid biomarker analyses

Analyses of the general sedimentary matrix of the MSA deposits in South African cave sites show that they contain a significant amount of organic material derived from terrestrial plants and trees ([Goldberg et al., 2009; Collins et al., 2017; Haaland et al., 2020; Wadley et al., 2020](#)). This organic material contains well-preserved lipid compounds derived from leaf epicuticular waxes, the wax coating covering the outer surface of the leaf cuticle in land plants ([Eglinton and Hamilton, 1967](#)). Despite the fact that plant waxes are omnipresent and abundant in many soils today, they are not preserved in all depositional settings and are susceptible to biodegradation. Hence it is not trivial to successfully establish a plant wax biomarker sequence from cave deposits. In 2019, 12 sediment samples were collected from the south wall vertical section at BBC for long-chain (C25-C33) *n*-alkane analyses ([Table 2; Figure 2](#)).

Organic geochemical and stable isotope analyses were performed at the organic geochemistry laboratory of Lamont Doherty Earth Observatory (LDEO) and the FARLAB stable isotope facility at University of Bergen (UiB). For this study, we analysed 12 samples that were extracted at semi-regular intervals from the section of the BBC sediment stratigraphy ([Table 2; Figure 2](#)).

Each sample was freeze-dried and homogenised using a mortar and pestle. Lipids were then extracted from each 13-41 gr sample with a 9:1 (v/v) solution of dichloromethane (DCM) and methanol using a Dionex 350 Accelerated Solvent Extractor (ASE). The resulting Total Lipid Extract (TLE) was dried under a stream of nitrogen gas in a Biotage TurboVap.

Compounds were next separated using activated silica gel flash column chromatography. Samples were sequentially eluted with

**TABLE 2** Sediment samples analysed for leaf wax *n*-alkane composition. List of the twelve sediment samples sampled and analysed in this study with sample number, stratigraphic provenance and depth, ages (based on Jacobs et al. (2020)) of the deposits. \*The CB horizon has not been OSL dated. Due to its stratigraphic vicinity to layer CA we use this age range for layer CB based on Jacobs et al., 2020.

Sample numbers	Stratigraphic Aggregate	Unit/Phase	Indicative modelled OSL age range (95.4% probability ka BP)	Concentration of total <i>n</i> -alkanes per gram of sediment ( $\mu\text{g/g}$ )
1	DUN	DUNE	73.7-62.9	0.64
2	CB*	M1	75.4-69.4	1.56
3	CC	M1	75.4-70.0	3.43
4	CD	M1	75.4-69.5	0.26
5	CFA	M2 Upper	77.4-71.9	1.14
6	CFB/CFC	M2 Upper	77.8-72.1	1.20
7	CGAA/CGAB	M2 Lower	84.1-75.9	n.d.
8	CGAC	M2 Lower	83.8-74.7	n.d.
9	CH	M3	90.8-80.5	1.93
10	CIBh2	M3	89.7-81.0	2.02
11	CJ	M3	98.2-85.2	4.68
12	CP	M3	95.8-85.5	n.d.

four bed volumes of hexane, DCM, and methanol to isolate the aliphatic, ketone, and polar fractions respectively. *n*-alkanes (in the aliphatic fraction) were identified and quantified using an Agilent 7,890 gas chromatograph equipped with a mass selective detector (MSD), flame ionisation detector (FID). Gas chromatography was performed with a 30m DB-5 capillary column. The GC oven was held at 60 °C for 1.5 min before the temperature ramp: first to 150 °C at a rate of 15 °C per minute, and then to 320 °C at 4.5 °C per second. We identified and quantified *n*-alkanes by comparing sample chromatograms to a commercially available standard containing C10-C40 homologues. Hydrogen isotope measurements were performed on a Thermo Trace GC coupled to a Thermo Delta V Isotope Ratio Mass Spectrometer (IRMS) via an Isolink Conflo IV interface. To convert compound-specific  $\delta^2\text{H}$  values to the VSMOW scale, we measured the authenticated A7 *n*-alkane mixture provided by Arndt Schimmelmann from the University of Indiana. The A7 was measured after 6 samples, at least. Each run was monitored for instrument drift with the A7 before calibration. Sample replicates were measured in separate runs and thus had separate calibrations for each run. Each sample was measured at least twice, and up to five times. The precision of replicate measurements was always better than 2.6‰ ( $1\sigma$ ). An *n*-alkane mixture (even *n*-alkanes only) was measured as an unknown control throughout the 5 runs, and  $\delta^2\text{H}$  precision was measured to 1.95‰ and 1.83‰ ( $1\sigma$ , N=10) for C30 and C32 respectively.

To assess the level of degradation of the plant waxes, we calculated the carbon preference index, CPI (Bray and Evans, 1961, (Supplementary Figure S2)). The CPI reflects the molecular distribution of odd-to-even *n*-alkanes within a specific carbon number range (here *n*-C21 to *n*-C33), (Herrera-Herrera et al., 2020). High CPI values (>5) indicate a significant contribution of waxes from terrestrial plants and low levels of degradation while low CPI values indicate low input of plant waxes from terrestrial plants or high degradation (Eglinton and Hamilton, 1967). The average

chain length ( $\text{ACL}_{21-35}$ ) was calculated following Poynter et al. (1989) to further help assess changes in vegetation (Supplementary Figure S2). Ratios between specific *n*-alkanes can be calculated as they are sensitive to environmental influences (e.g., Schefuß et al., 2003; Carr et al., 2014). The ratio of the *n*-alkane homologues C29 and C31 was used to calculate the Norm31 index (Supplementary Figure S2); (e.g., Carr et al., 2014). Using this index together with the general *n*-alkane distribution patterns can reveal the differences between plant types, and their affinity to distinct biomes. In South Africa, soils with the highest ACL and Norm31 values have been found in the arid-adapted Succulent Karoo biomes, followed by Nama Karoo. Soils with lower Norm31 index were attributed to more humid-adapted biomes such as Grassland, Savanna and Fynbos (Carr et al., 2014; Herrmann et al., 2016).

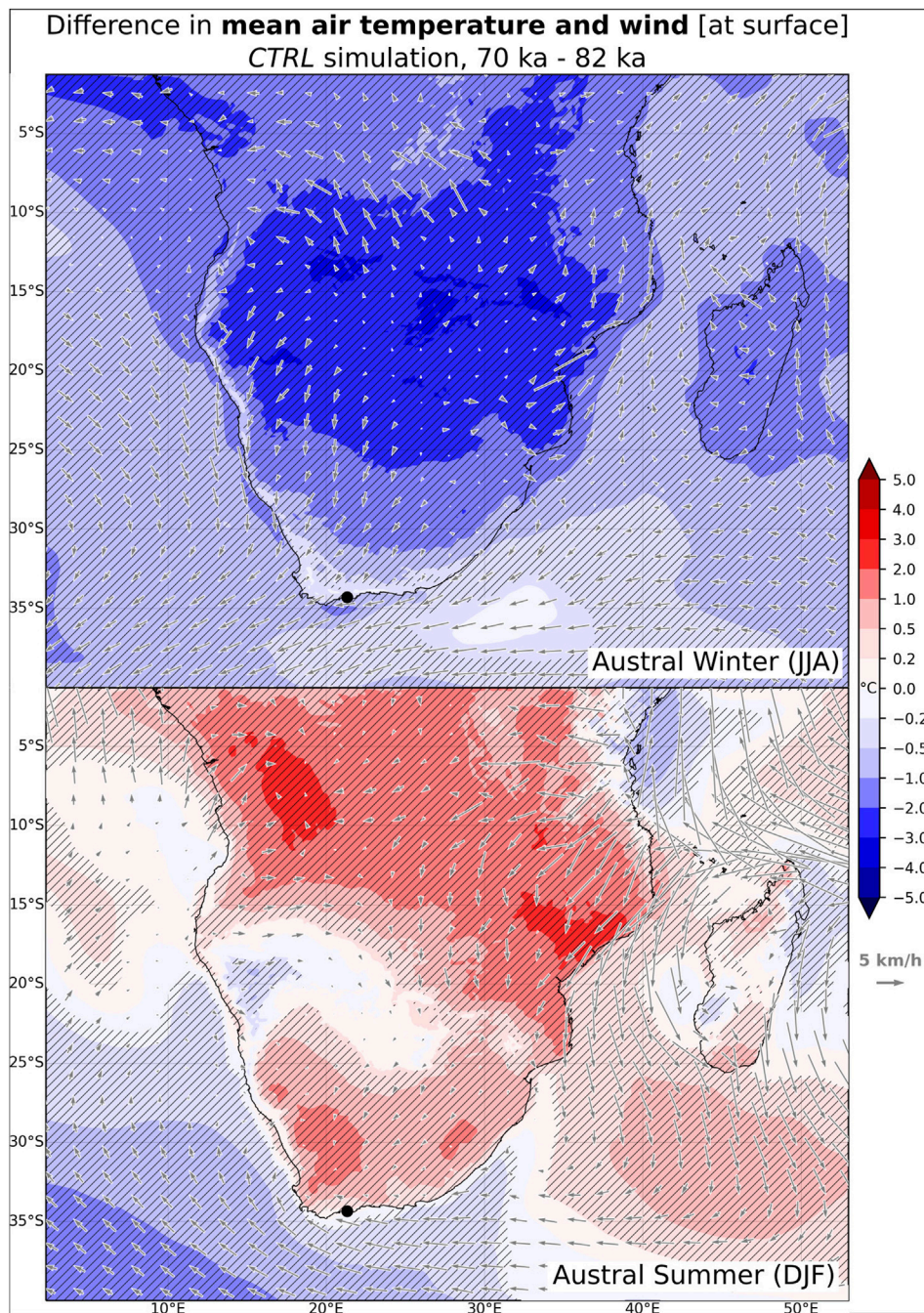
## 4 Results and discussion

### 4.1 Modelled climate change in southern Africa from 82 to 70 ka

Climate change in southern Africa from 82 to 70 ka was assessed by analyzing the output from the 4 WRF simulations (Table 1), namely, the control (CTRL) and the exposed land (*ExpLand*) runs for each of the two epochs.

#### 4.1.1 Large-scale changes

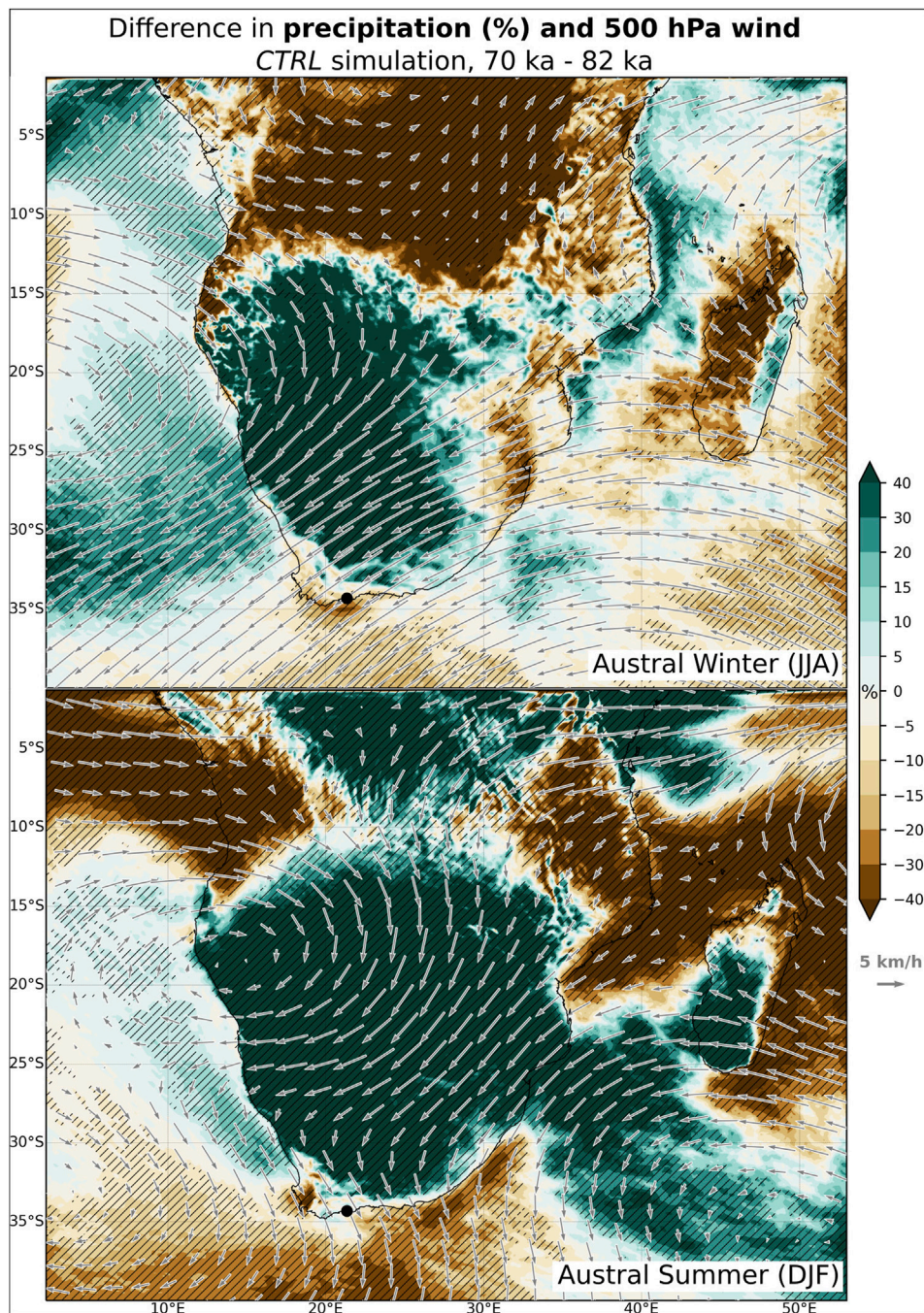
Several significant large-scale changes are observed from 82 to 70 ka. For instance, seasonality over land is more pronounced at 70 ka, with up to 4 °C higher (lower) mean surface air temperatures during austral summer (winter) compared to 82 ka (Figure 3). Widespread increases in rainfall during summer are also evident (Figure 4). Summer warming over land areas occurs despite the

**FIGURE 3**

Change in 30-year mean surface air temperature and surface winds from 82 to 70 ka (CTRL simulation). Top: Austral winter (JJA). Bottom: Austral summer (DJF). Statistically significant differences in temperature (*t*-test, 95% confidence level) are hatched. Present day coastline is plotted, and the Blombos Cave location on the southern African coast is indicated with a small dot.

cooling effects of increased cloudiness and evaporation (not shown), as well as from the higher overall elevation (caused by the lower sea level) at 70 ka (Göktürk et al., 2023). These epochal differences in temperature and precipitation are mainly associated with an increase (decrease) in summertime (wintertime) insolation from 82 to 70 ka, owing to a half-period advance of the orbital precession cycle (Thompson et al., 2005). The accompanying free troposphere (500 hPa) changes feature anomalous northerly and easterly flows

(with respect to 82 ka) south of 20°S (Figure 4), which indicate enhanced monsoon circulation and increased moisture transport into southern Africa from the tropics and the Indian Ocean during summer at 70 ka. The southern boundary of the wetter area during summer (Figure 4) is located roughly where the anomalous northeasterly flow is replaced by a northwesterly flow from the cooler Atlantic Ocean, highlighting the role of the large-scale circulation influence on surface climate. There are precipitation

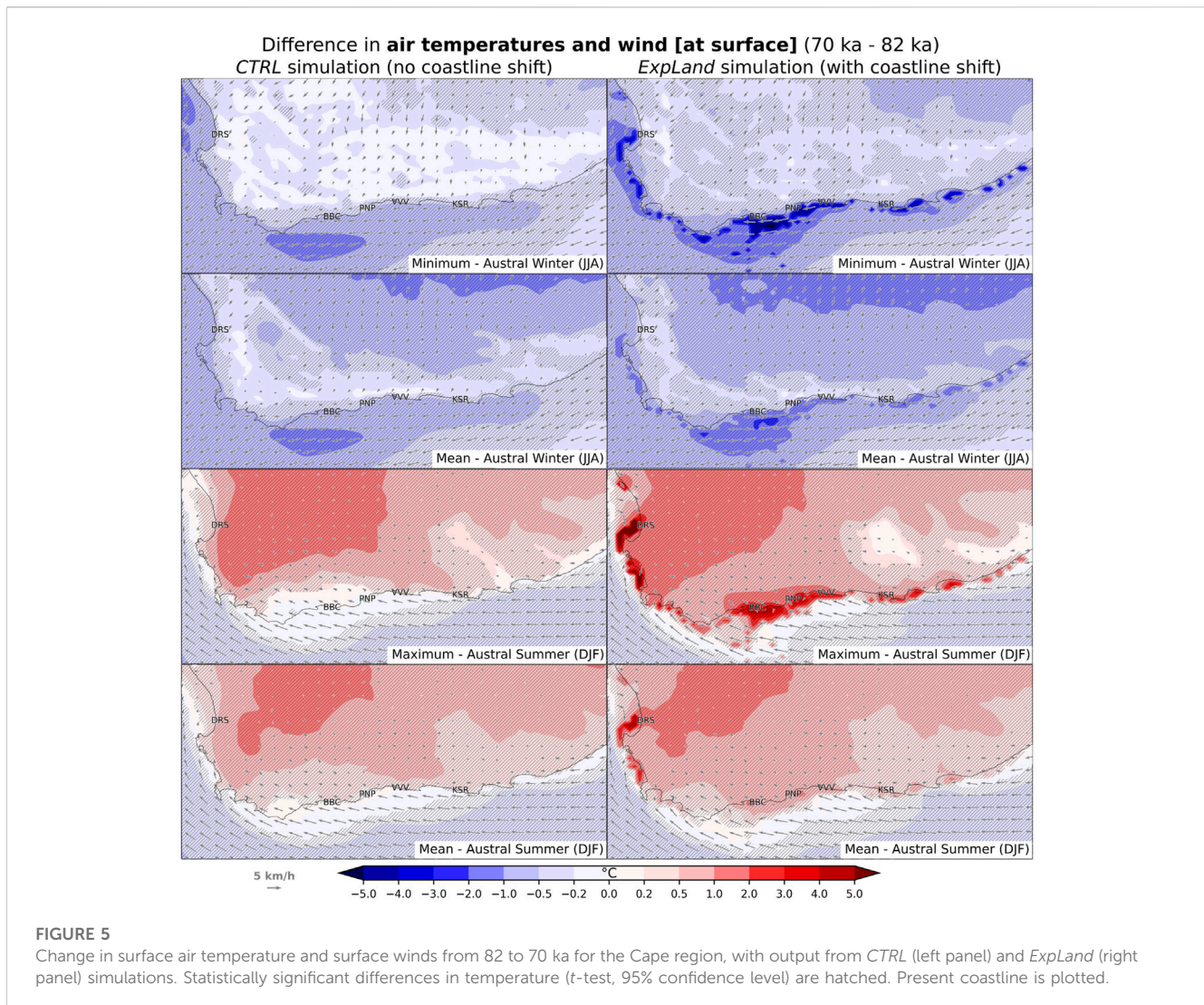
**FIGURE 4**

Change in 30-year mean precipitation (as percentages) and 500 hPa winds from 82 to 70 ka (CTRL simulation). Top: Austral winter (JJA). Bottom: Austral summer (DJF). Statistically significant differences in precipitation (t-test, 95% confidence level) are hatched. Present day coastline is plotted, and the Blombos Cave location on the southern African coast is indicated with a small dot.

increases at 70 ka over inland southern Africa in winter too, though they occur largely in the winter-dry region, thus are generally small in absolute values.

Over the oceans, difference patterns in mean temperature and precipitation are broadly compatible with SST changes. SSTs are generally lower at 70 ka around the continent, for instance with an Agulhas Current that is locally more than 2 °C cooler than at 82 ka off the coast of southwestern Cape region in winter (Supplementary

Figure S1). Weaker westerlies (Figure 4), as well as the aforementioned drop in SSTs at 70 ka lead to reductions in rainfall of up to 40% over the ocean off the southern Cape during winter (Figure 4), compared to 82 ka. In similar fashion, rainfall reductions (up to 40%) are simulated over the Indian Ocean off the south eastern Cape coast at 70 ka in summer, when the Agulhas Current is 0.5°C–1 °C cooler than 82 ka. This is in stark contrast with the increasing summer temperatures and rainfall



inland, where higher insolation at 70 ka controls the pattern of change (Figure 4).

Overall, large-scale differences between 70 and 82 ka are dominated by insolation-driven changes over land and SST-driven changes over the ocean.

## 4.1.2 Regional and local climatic changes over coastal southern Africa

### 4.1.2.1 Excluding coastline shifts (*CTRL* simulations)

Between 82 and 70 ka the southern coastal strip of the Cape region was affected by climatic changes that occurred both inland and over the ocean. These are explained in the previous section. Our control (*CTRL*) simulations used the present coastline for both of the epochs (i.e., local changes to the coastline in response to glacial sea level variations are not taken into account), therefore they are a good means for analysing the influence of large scale changes (ocean and inland) on coastal southern Africa, while excluding the effects of the coastline shift. For example, there is modest but statistically significant ( $0.5^{\circ}\text{C}$ - $1^{\circ}\text{C}$ ) winter cooling at 70 ka along the southwestern Cape coast (where BBC is located) in our *CTRL* simulation (Figure 5, left panel), and this seems to be a result of

the decrease in air temperatures over the adjacent ocean. Conversely, the change in summer temperatures without the coastline shift is small and not significant (Figure 5, left panel), since the coastal strip is situated approximately halfway between a relatively warmer land and a cooler ocean during summer at 70 ka compared to 82 ka. Likewise, in summer, there is no significant precipitation change for the southwestern Cape coast, as the region is well south of the southern boundary of the inland rainfall increase, also far from the ocean area off the southeastern Cape where there is less rainfall at 70 ka (Figure 6, left panel). However, the reduction in rainfall during the cooler season (from May to September) is significant (15%-20%), even when the coastline shift is excluded (Figure 7; Figure 8). This is in response to both lower SSTs off the southwestern coast and weaker winter westerlies at 70 ka.

### 4.1.2.2 With coastline shifts (*ExpLand* simulations)

A large area of land adjacent to the present coastline, called the palaeo-Agulhas Plain, was exposed at 70 ka as a result of the falling sea level (Figure 1). This shifted the coastline  $\sim 30$  km south of its 82 ka position near BBC. The exposed land (*ExpLand*) simulation in our study takes into account this land expansion and the associated

Difference in **precipitation (%)** and **surface wind (70 ka - 82 ka)**  
**CTRL simulation (no coastline shift)**      **ExpLand simulation (with coastline shift)**

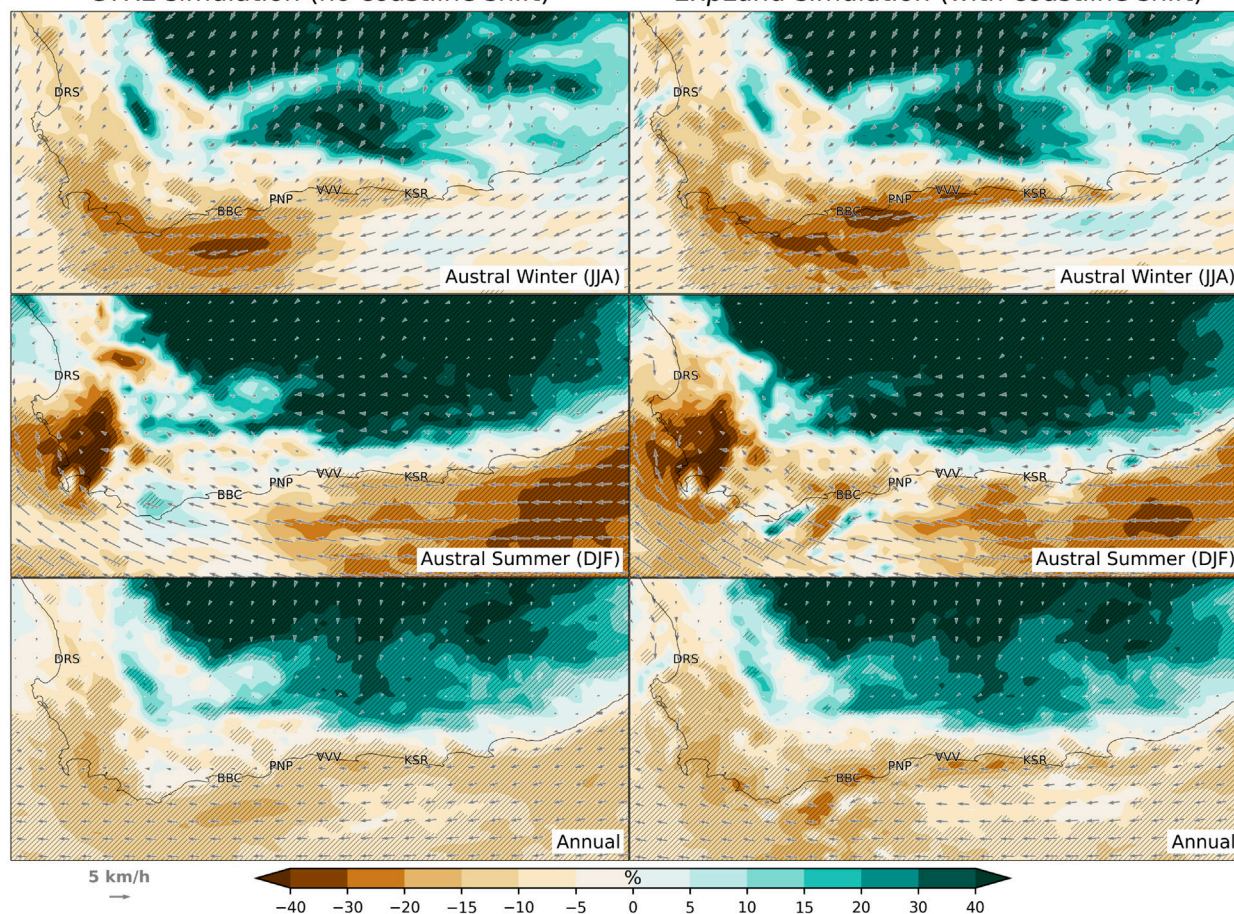


**FIGURE 6**

Change in 30-year mean precipitation (%) and surface winds from 82 to 70 ka for the Cape region, with output from CTRL (left panel) and ExpLand (right panel) simulations. Statistically significant differences in temperature (t-test, 95% confidence level) are hatched. Present coastline is plotted.

coastline shift by using distinct coastlines in each of the 82 and 70 ka runs, instead of using the modern coastline in both. Modelled climate change in the region arising purely from an estimated coastline shift was found to be substantial, leading to a more continental climate for locations that were previously coastal (Göktürk et al., 2023).

The coastline shift that occurred between 82 and 70 ka also caused significant local climatic shifts in the southern Cape region, as revealed by our ExpLand simulation. For instance, in the BBC area, cooler nights and warmer days were simulated for all months at 70 ka compared to 82 ka (Figure 7), but they are not necessarily associated with a shift in the daily mean temperature. However, any change in daily minimum or maximum temperatures in the CTRL simulation are much smaller, and they always occur in the same direction in any given month and only when there is a change in the mean temperature (Figure 5; Figure 13). This shows that the year-round cooler nights and warmer days at 70 ka are mainly caused by the exposed land altering surface radiative properties and inducing a more continental diurnal range of temperatures. The most striking change contributing to this new temperature regime at 70 ka is the

2°C–4°C rise in summer daily maximums, which spreads well inland due to a weakening of the sea breeze (Figure 5, right panel). Since this daytime warming is stronger than the night-time cooling in the warm season, there are significant increases (up to 1°C near BBC) in summer mean temperatures as well. Also significant in the ExpLand simulation is the night-time cooling (~2°C at Blombos) in winter, which amplifies the large-scale winter cooling signal already present in the CTRL simulation (Figure 5). Differences in mean temperatures during fall and spring are insignificant, as neither daytime warming nor night-time cooling dominates during the transition seasons (not shown). The regime shift in temperatures is also evident from the analysis of a few climate indices in the ExpLand simulation. From 82 to 70 ka, the mean annual number of days with a maximum temperature of at least 25°C (summer days) rises from 7 to 40, while those with a minimum of 5°C or below increase from 9 to 30 (Figure 10). Days with such low or high temperatures are very rare in the BBC area in our CTRL simulation, at both epochs (with long-term averages less than 1 day per year, Figure 10), which again demonstrates the climatic significance of the exposed palaeo-Agulhas Plain. Overall, both the diurnal and the

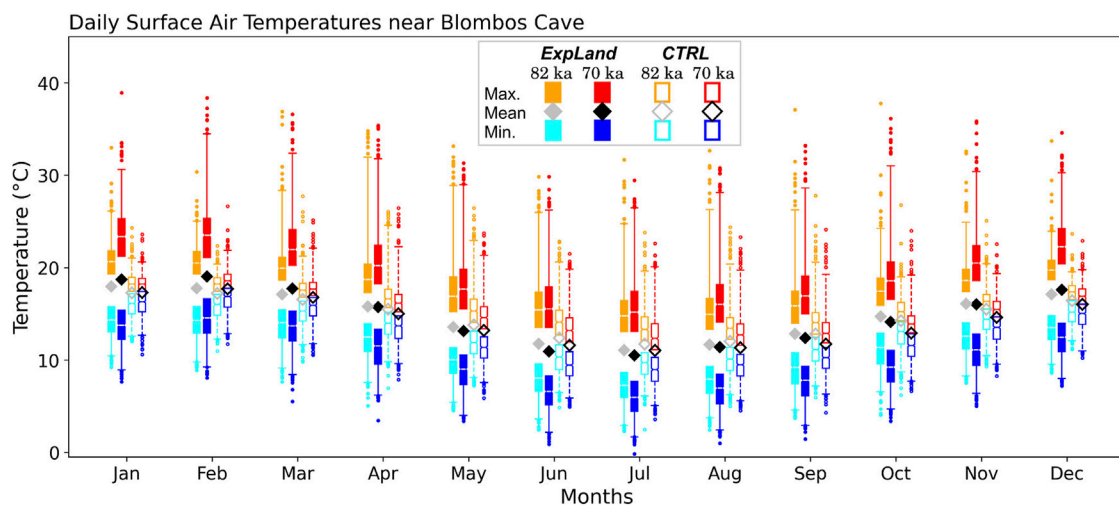


**FIGURE 7**

Daily maximum, minimum and mean surface air temperatures at around Blombos Cave locality through the 30-year simulation periods of WRF model at 70 and 82 ka. Only the long-term monthly averages are shown for daily means, whereas daily extremes are summarized as box-and-whisker plots. For the sake of clarity, lower (upper) whiskers for maximum (minimum) temperatures were removed. Outliers shown belong to the 99th (1st) percentile of daily maximums (minimums).

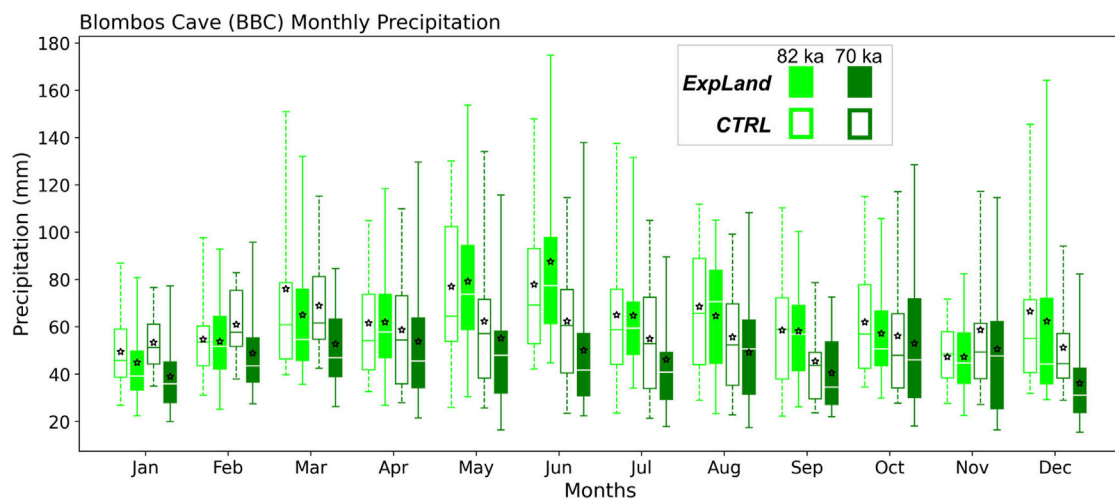


**FIGURE 8**

Monthly precipitation amounts at around Blombos Cave locality through the 30-year simulation period of WRF model at 70 and 82 ka. Stars are the 30-year mean values. Outliers (beyond 99th and 1st percentiles) are not shown.

annual range of temperatures become greater at 70 ka due to the coastline shift (Figure 13), reinforcing the large-scale effects arising from orbital forcing.

As noted previously, our CTRL simulation does not show any considerable change in precipitation amounts over the southern Cape coast for the warm half of the year, but it indicates 15%–20% less rainfall from May to September (Figure 8) due to weaker westerlies and a cooler Agulhas Current at 70 ka (Figure 6, left panel). The exposed land around the region at 70 ka causes additional, year-round reductions in precipitation by weakening

near-surface winds through increased drag (Figure 6, right panel), thus allowing less moisture from the ocean into the BBC area, which is now located inland. Winter rainfall reduction in the ExpLand simulation is over 30%, while summer rainfall also decreases by at least 20%. Annually, there is 20%–25% less precipitation at 70 ka compared to 82 ka (Figure 6, right panel). The decline in the rainfall amounts is accompanied by significant changes in rainy days count and dry spell length over the region (Figure 9). For instance, in the BBC area, there are 21 fewer days annually

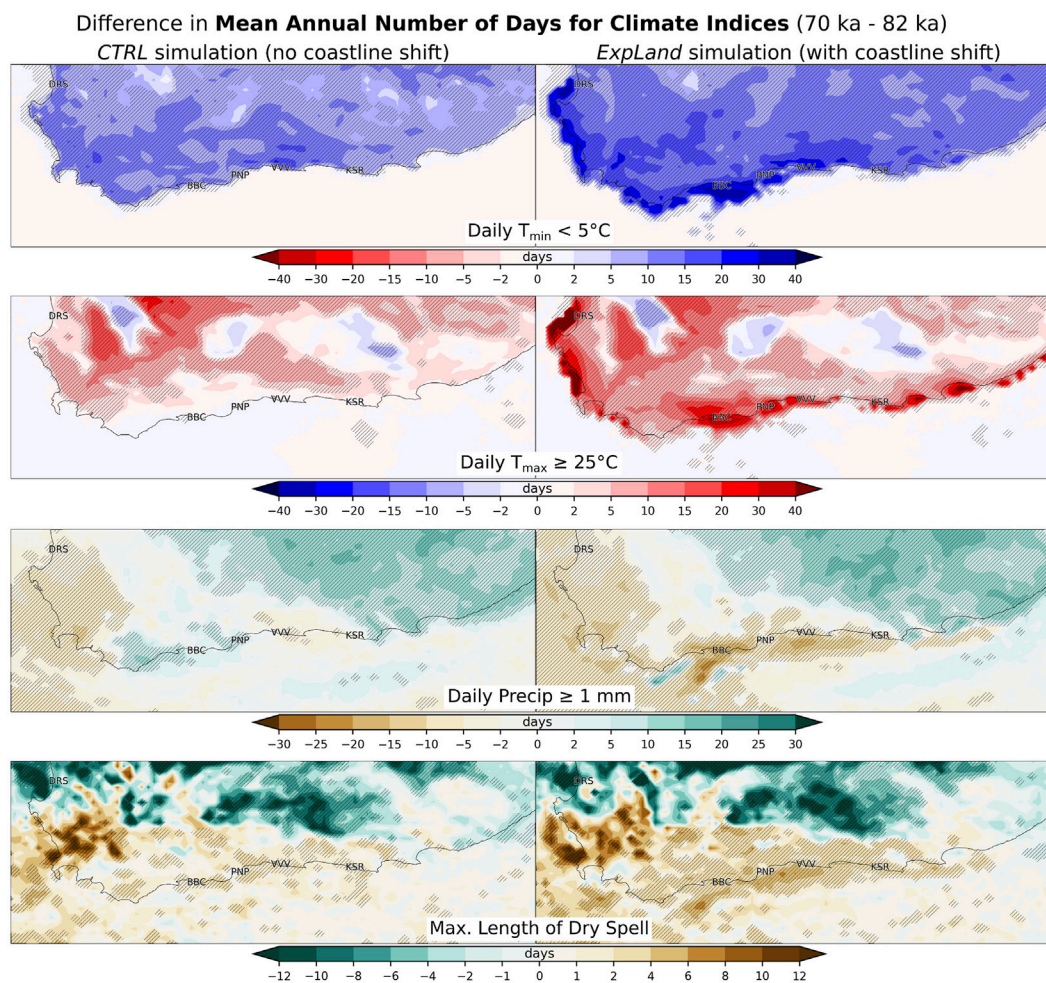


**FIGURE 9**

Change in the 30-year average annual number of days for some climate indices from 82 to 70 ka for the Cape region, with output from CTRL (left panel) and ExplLand (right panel) simulations. Statistically significant differences (t-test, 95% confidence level) are hatched. Present coastline is plotted.

with at least 1 mm of rainfall, and the maximum length of dry spells within a year is longer by 4.6 days on average (Figure 10). It is worth noting that, when the coastline shift is *not* considered (CTRL simulation), the mean annual number of wet days *increases* slightly at 70 ka in the BBC area (Figure 10), strongly suggesting that the lower number of rainy days in the ExplLand simulation is mainly due to the coastline shift. The change in precipitation-evaporation differences from 82 to 70 ka confirms the robust drying signal (Figure 11). Statistically significant decreases in this parameter are observed for both winter and summer, also annually, with a stronger drying in winter which fits the greater reduction in winter precipitation amounts. Higher daytime temperatures in summer probably also play a role in summer drying by enhancing evaporation.

To conclude, the expansion of land at 70 ka reduces the amount and frequency of rainfall, and increases the diurnal and interseasonal temperature ranges around the BBC area, compared to 82 ka. This, and the contribution from other, larger-scale factors explained in the previous section, lead to a significantly drier and more continental climate in the BBC area at 70 ka.

## 4.2 Local long-term climate changes at BBC as inferred from leaf wax *n*-alkanes

### 4.2.1 Leaf-wax content, distribution and preservation

The BBC samples contained plant wax-derived *n*-alkanes with chain lengths ranging from C21 to C35 carbon atoms (Figure 12). Their concentrations and elevated CPI values (4.5–16.5, with an average of 9.8) in all samples document moderate input of non-degraded plant-waxes (Supplementary Figure S2). The C31 *n*-alkane was consistently the most abundant compound in all samples with the C33 *n*-alkane being the second most abundant homologue. Leaf wax *n*-alkane concentrations are highly variable; they exhibit a range from 0.1 to 1.87  $\mu\text{g g}^{-1}\text{ dw}$  (for the C31 *n*-alkane) and as such are similar to present day Lowland Fynbos soils (0.4–5.6  $\mu\text{g g}^{-1}\text{ dw}$ ), (Herrmann et al., 2017). Three sampled layers: CP (M3 unit), CGAC and CGAA/CGAB (M2 lower unit) yielded insufficient *n*-alkanes for analysis (Table 2).

Leaf-wax  $\text{ACL}_{21-35}$  exhibit stable values with an average of 30.2 ( $\pm 0.2$ ), (Supplementary Figure S2). Norm31 values are variable and

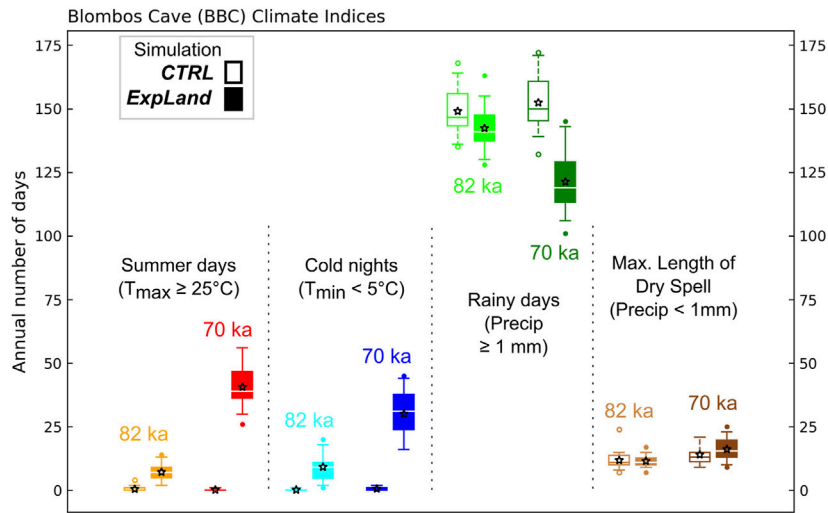


**FIGURE 10**  
Annual number of days for some climate indices at Blombos Cave area at 82 to 70 ka, with output from CTRL and ExpLand simulations. Stars are 30-year averages. Outliers are the values beyond 1st and 99th percentiles.

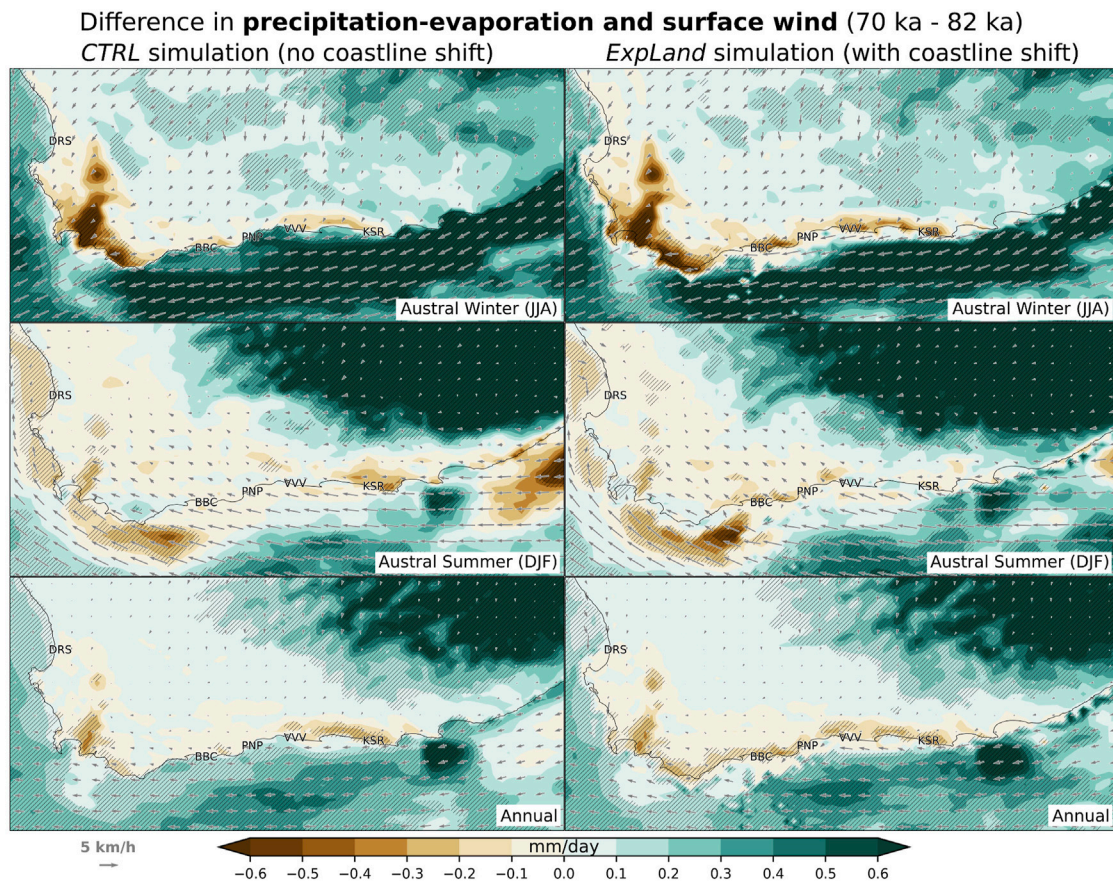


**FIGURE 11**  
Change in 30-year mean precipitation minus evaporation values, and surface winds, from 82 to 70 ka for the Cape region, with output from CTRL (left panel) and ExpLand (right panel) simulations. Statistically significant differences (t-test, 95% confidence level) are hatched. Present coastline is plotted. Note that the values on the exposed land areas at 70 ka are masked.

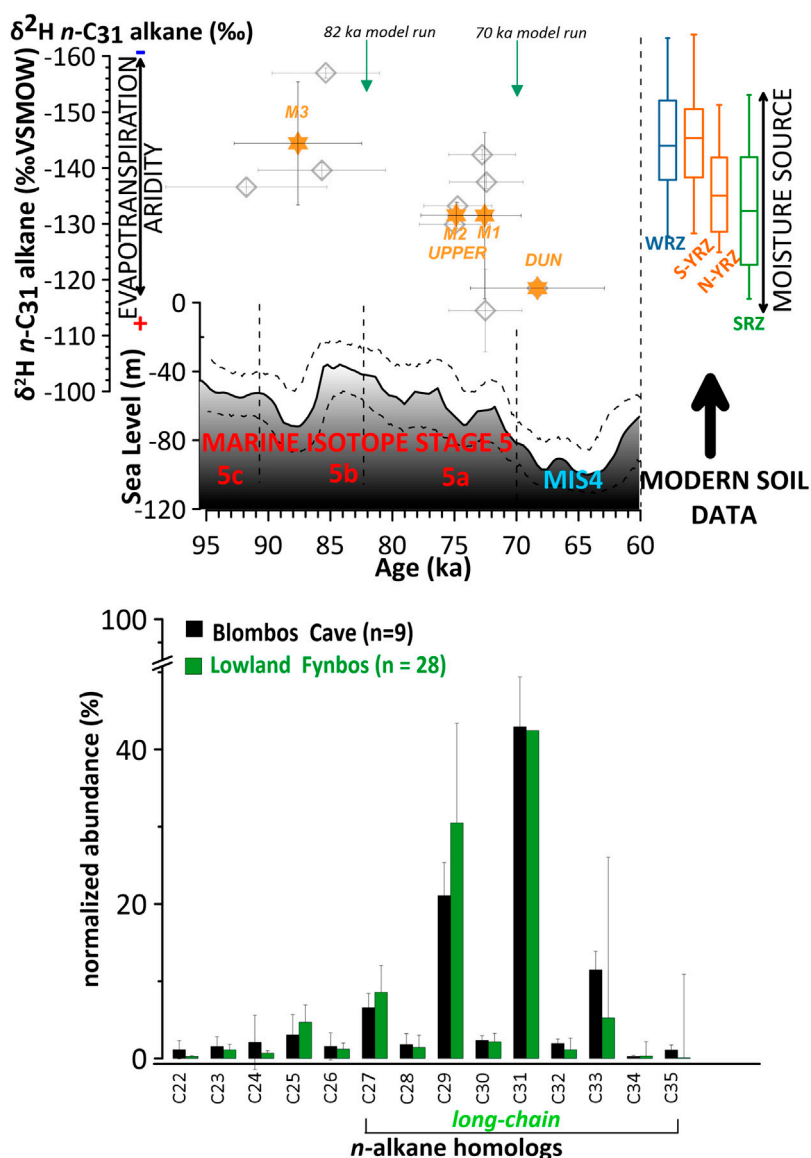


**FIGURE 12**

Palaeoenvironmental proxy evidence from BBC derived from leaf wax *n*-alkane study. Upper panel: Hydroclimate indications based on leaf wax *n*-alkane  $\delta^2\text{H}$  (grey diamonds) against global sea-level record (Grant et al., 2012) with lower and upper 95% confidence limits. Data is plotted on the latest Bayesian modelled OSL chronology for the cave (Jacobs et al., 2020) (horizontal errors,  $2\sigma$ ) and results are based on replicate  $\delta^2\text{H}_{\text{wax}}$  measurements (vertical errors,  $2\sigma$ ). Orange stars are  $\delta^2\text{H}_{\text{wax}}$  mean values (averaging individual grey diamond values) for archaeological phases as indicated in Figure 2 (DUNE, M1, M2 UPPER, M3). Modern soil reference data for rainfall zones indicate moisture source changes (Winter Rainfall Zone (WRZ) (Herrmann et al., 2017), Summer Rainfall Zone (SRZ) (Herrmann et al., 2017), southern (S) and northern (N) Year-round Rainfall Zone (YRZ) (Strobel et al., 2020). Stratigraphical position of climate model run time slices at 82 ka and 70 ka are highlighted as green arrows. Marine Isotope Stages are indicated. Lower panel: *n*-alkane concentrations per sample in % abundance averaged over 9 samples (errors  $2\sigma$ ), displaying a Fynbos-like distribution (dominance of C31 and C29) (Carr et al., 2014).

range between 0.64 and 0.76 with an average of 0.68 ( $\pm 0.4$ ) (Supplementary Figure S2). Throughout the sequence the ACL and CPI values display no overall trend (Supplementary Figure S2). The ACL-CPI cross plot reveals that values of the BBC samples differ significantly from samples from burning experiments of Wiesenberg et al. (2009) as they fall within the range of unburnt straw and soils. As such, we conclude that heating/burning has left no impact on our samples or that the plants were not heated or burned in those layers (Supplementary Figure S2).

Hydrogen isotope composition ( $\delta^2\text{H}_{\text{wax}}$ ) values of the *n*-C31 *n*-alkane range throughout the MSA sequence in BBC from  $-114\text{‰} \pm 7.4$  to  $-157\text{‰} \pm 0.9$  (Figure 12). There is significant inter-layer  $\delta^2\text{H}_{\text{wax}}$  variability within depositional units (Figure 12). Samples from unit M2: CGAC and CGAA/CGAB yielded *n*-alkane abundances too low for reliable  $\delta^2\text{H}$  determination. All reported plant-wax data are available in our Supplementary Material.

The distribution of long-chain (C27-C33) compounds indicates that *n*-alkane homologs predominantly derive from terrestrial

vegetation with all samples closely resembling the average of modern Lowland Fynbos vegetation (an evergreen, sclerophyllous shrub) (Figure 12); (Carr et al., 2014). Throughout the sampled sequence ( $91.8 \pm 6.5$ – $68.3 \pm 5.4$  ka), no overall trend in Norm31, ACL and CPI indices and *n*-alkane chain length distribution occurs (Supplementary Figure S2). This might imply that no significant vegetation changes occurred over time in the area surrounding BBC. Given the known climate changes driven by orbital and SST forcing and the strong local changes arising from sea level drop suggested by the regional model, the lack of variation in vegetation type might indicate that the collecting habits of the inhabitants were biased towards collecting the plants resembling the modern Fynbos biome despite changing climate conditions and vegetation around the cave. However, this assumption requires further investigation.

The samples analysed from the M3 phase (CP, CJ, CIBh2 and CH) consisted of the lowest and oldest parts in the MSA section of BBC and are dated to fall within MIS 5c/b. The  $\delta^2\text{H}_{\text{wax}}$  values in M3 range from  $-137\text{‰} \pm 1.4$  for layer CJ; the most depleted values in the record are  $-157\text{‰} \pm 0.9$  for layer CIBh2 and values of  $-140\text{‰} \pm 1.4$  in layer CH, the youngest in the M3. The averaged value (orange star) for the M3 phase ( $n=3$ ) is  $-144\text{‰} \pm 11$ , (Figure 2; Figure 11). The two samples from the Upper M2 phase (dated to MIS 5a), layers CFB/CFC and CFA, had stable values of  $-130\text{‰} \pm 2.6$  and  $-133\text{‰} \pm 0.6$ , respectively. The phase's average is  $-132\text{‰} \pm 2.3$ . The  $\delta^2\text{H}_{\text{wax}}$  values in the M1 phase range from  $-115\text{‰} \pm 7.4$  in the CD layers, the lowest (oldest in that phase) to  $-142\text{‰} \pm 0.9$  in the CC layer and  $-138\text{‰} \pm 1.2$  in the layer CB. The latter sample is positioned on top of the phase stratigraphically sitting at the MIS 5a/4 transition. The phase's mean average is  $-131\text{‰} \pm 14.9$ . Positioned at the boundary between CA and the dune layer (MIS 4) the  $\delta^2\text{H}_{\text{wax}}$  value for the youngest sample analysed in the sequence is  $-119\text{‰} \pm 1.9$ .

The range of  $\delta^2\text{H}_{\text{wax}}$  values throughout the sequence is in line with the contemporary soil samples from the YRZ (Herrmann et al., 2017; Strobel et al., 2020) suggesting that sedimentary  $\delta^2\text{H}$  is representative of the mean  $\delta^2\text{H}$  of vegetation from the region surrounding the cave.

#### 4.2.2 Leaf wax *n*-alkane results and implications for climate

Increasing  $\delta^2\text{H}_{\text{wax}}$  values throughout the sequence suggest a shift in hydroclimate at BBC from MIS 5c/b to glacial MIS 4 with a coeval drop in sea level (Figure 12). The interpretation is not dependent on ice volume correction of seawater  $\delta^2\text{H}$ , which means, applying a correction for global ice volume changes on the proxy record does not change the observed pattern. Correcting for global ice volume ( $\sim 8\text{‰}$   $\delta^2\text{H}$  enrichment of seawater from increased global ice volume during glacial periods (Duplessy et al., 2002)) is common practice in paleowater isotope studies. However, it assumes that the same net change is experienced everywhere on the planet. This view was recently challenged (Windler et al., 2020).

One way to interpret these changes is as a decrease in precipitation amount over time (Sachse et al., 2012) in the landscape surrounding BBC. Reduced overall rainfall amounts would lead to an enrichment process by which the relative abundance of the heavier isotope increases, making  $\delta^2\text{H}$  of rainfall more positive. When it is drier,  $\delta^2\text{H}$  is more enriched as

raindrops evaporate more in a drier atmosphere (Dansgaard, 1964). Evapotranspirative enrichment of leaf water is an additional driver of  $\delta^2\text{H}_{\text{wax}}$ . Changes in regional climate which alter the balance between precipitation and evapotranspiration can also influence the  $\delta^2\text{H}_{\text{wax}}$  signal (Schefuß et al., 2005), with higher values suggesting increased evapotranspiration associated with long, dry summers, i.e., higher surface air temperatures in southern South Africa and/or lower relative humidity.

Alternatively, the  $\delta^2\text{H}_{\text{wax}}$  signal could be interpreted as changing rainfall seasonality contributing precipitation from different moisture sources (Figure 12). Southern Africa is characterized by large differences in the isotopic composition of precipitation. Rainfall brought by the westerlies in winter is more depleted in  $\delta^2\text{H}$ , while it is more enriched when brought in via easterlies in summer (Harris et al., 2010; Braun et al., 2017). It should be noted that the modern-day intra-zonal values of the southern-YRZ (Figure 12) are large and overlap with the range of  $\delta^2\text{H}_{\text{wax}}$  values for the SRZ. This makes it challenging to determine whether the  $\delta^2\text{H}_{\text{wax}}$  data indicate a trend towards proportionally more summer precipitation or more uniform rainfall throughout the year, as time progresses.

We view the possibility that the shift in values may reflect input of more shrub-like vegetation rather than grasses as unlikely. This is because the input of more shrub-like vegetation rather than grasses throughout the sequence, is not consistent with the  $\text{CPI}_{25-33}$ ,  $\text{ACL}_{21-35}$  and Norm31 indices reconstructions; that is, throughout the sampled sequence ( $91.8 \pm 6.5$ – $68.3 \pm 5.4$  ka) no overall trend in these indices occurred (Supplementary Figure S2). Supporting this is the micro-mammal reconstruction from BBC which indicates that shrubland oscillated, with the greatest abundance associated with the M3 phase and an overall decline towards MIS 5b/a in the sequence (Nel and Henshilwood, 2021).

Due to the lowering of the sea-level over time, the relative position of the BBC with regards to ocean moisture sources changed. Elevation difference can influence rainfall  $\delta^2\text{H}$  signatures which become deuterium-depleted with altitude (ca. 10%–15% per 1,000 m; Gonfiantini et al., 2001). However, the change in altitude is too small for this effect to be significant (<100 m, i.e. 1–1.5‰ deuterium depletion), and the trend in the  $\delta^2\text{H}_{\text{wax}}$  signal over time is the opposite of what would be expected due to the altitude effect on deuterium.

#### 4.3 Data-model comparison and constraining the leaf-wax *n*-alkane proxies

In order to constrain the multiple factors that can influence the  $\delta^2\text{H}_{\text{wax}}$  signal, we compare our leaf wax *n*-alkane data with the modelling experiments. Our modelling results for the BBC area indicate that at 70 ka compared to 82 ka there are: 1) year-round, significant reductions in rainfall amounts (Figure 7 and Figure 8); 2) a lower number of rainy days (Figure 10); 3) lower values of precipitation minus evaporation (Figure 11) as a result of reduced precipitation (Figure 6) and significantly higher summer daytime temperatures (Figure 5) at 70 ka. These consistent and robust findings provide ample support for the interpretation of more enriched  $\delta^2\text{H}$  values of leaf wax *n*-alkane as a year-round terrestrial drying signal as well as a transition to a more continental climate

from 82 to 70 ka (Figure 12). Less precipitation counterbalances the amount effect, and increasing summer warmth leads to evaporative isotopic fractionation of soil moisture, both of which push  $\delta^2\text{H}_{\text{wax}}$  towards less negative values. This pattern may also be enhanced by changes in rainfall seasonality between 82 and 70 ka. The percentage decline in winter precipitation (with more depleted isotopic values) is somewhat greater than that in summer in our model output. Winter rainfall accounts for 29% of total annual precipitation at 82 ka but declines to 25% at 70 ka, while summer rainfall stays at 21% of the total in both time slices. However, the role of changing precipitation seasonality in determining Blombos  $\delta^2\text{H}_{\text{wax}}$  values is probably relatively minor compared to that of the year-round drying evident in the modelling results.

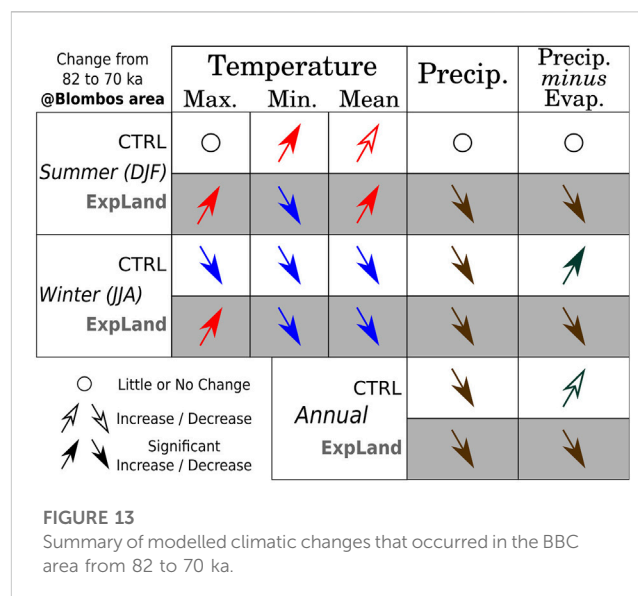
Despite that only nine individual data points are presented in this study, the mean values (orange stars in Figure 12) from the corresponding archaeological phases described (M3, M2 UPPER, M1, DUNE) are significantly different from each other. This is compatible with the interpretation that the progressively enriched  $\delta^2\text{H}_{\text{wax}}$  values result from increasing terrestrial aridity. Our interpretation is supported by stable carbon and oxygen isotope data of contemporaneous ostrich eggshells (OES) from BBC (Roberts et al., 2016), a record which also suggests increasing aridity with falling sea-levels. Data from nearby coastal archaeological sites (Figure 1) and lake records imply that this drying trend may have occurred along much of the southern Cape coast, as is also supported by our regional modelling results. The leaf-wax isotopic composition measured at Diepkloof Rock Shelter (DRS) (Collins et al., 2017) in the WRZ, when based on the Tribolo et al. (2013) chronology, suggest that MIS 5 (128–71 ka) was less arid, while MIS 4 (70–60 ka) was more arid. Further, multiproxy evidence from lake Vankervelsvlei (Strobel et al., 2022), a wetland located on the southern Cape coast in the YRZ of South Africa, was interpreted as increasing coastal aridity towards more glacial conditions with sea-level fall, akin to what happened from 82 to 70 ka.

Overall, the palaeoenvironmental data from the BBC MSA sequence combined with the regional modelling evidence point towards increasing terrestrial aridity from ~100 ka to 68 ka as the climate shifted alongside sea level variations.

#### 4.4 Environmental changes at BBC in the context of site usage, subsistence strategies and behavioural development

Understanding the emergence of modern human behaviour in South Africa requires analyses of a number of factors including climate, ecology and environment (Vahdati et al., 2019). Previous studies along the southern coast of South Africa proposed that sea-level change likely played an important role in human social, demographic and subsistence responses (Marean et al., 2020). While these studies have focused on the emergence of land due to isostatic sea level fall, and the consequent availability of a productive foraging landscape, our work quantitatively evaluates the consequences of the emerging Palaeo-Agulhas plain for local climate through time.

Fluctuating coastlines during the MSA at BBC probably affected the lives of coastal cave inhabitants in multiple ways,



as their access to the sea and marine resources changed substantially (Langejans et al., 2012). When the coastline was close to the cave, a situation occurring during interglacials, people had easy access to the ocean and likely fed on abundant and predictable shellfish resources (Marean et al., 2010). This way of coastal occupation is often associated with coastal hunter-gatherer communities (Yesner et al., 1980)—a logistical subsistence pattern where people are able to settle in the area longer due to increased food security (Whallon, 2006). A coastline retreat, on the other hand, exposed a sizeable land area off the southern coast of southern Africa: the so-called Palaeo-Agulhas Plain. This could have favoured the emergence of a large mammal ecosystem, supported hunting techniques that were more terrestrially adapted, and led to the development of more sophisticated toolkits (Marean, 2014; Marean et al., 2014; Copeland et al., 2016; Haaland et al., 2020; Venter et al., 2020).

Haaland et al. (2020) argue that the fluctuating coastline was the main driver for changes in regional site use and settlement dynamics at BBC. The periods in time that overlap with the most significant sea-level lowering and coastline retreat around South Africa are the MSA phases that indicate the most significant cultural and technological development (i.e., the Still Bay, stratigraphically dated to M1 and M2 Upper unit at BBC (Henshilwood et al., 2018; Haaland et al., 2020)). Geoarchaeological evidence suggests that during these periods human occupation was more frequent, but short-term (Haaland et al., 2020). Conversely, in the older MSA phase in BBC (i.e., the M3), the material culture is less varied and more uniform, and higher amounts of shellfish remains were found (Langejans et al., 2012). This suggests that intensive marine resource exploitation is associated with a longer-term occupation subsistence pattern (Haaland et al., 2020). Based on our new palaeohydrological proxy observations from leaf wax *n*-alkane patterns and the results of our regional climate modelling experiments, we conclude that more humid conditions were associated with the M3 unit and aridity increased towards and throughout the M1 Unit and associated Still Bay production (Figure 12).

## 4.5 Connecting changing environmental conditions with changes in behaviour

While fluctuating coastlines had a direct impact on the mode of coastal occupation and resource availability, we show here that they also changed the climate around the BBC site and along the present-day coast. Our model simulations suggest that the local climatic effect of the seaward coastline shift through the 82-70 ka transition was at least as substantial as that of large-scale drivers. This probably resulted in additional - and hitherto overlooked - climatic pressures and changes, which might have played a role in shaping the cultural and technological developments recorded in the BBC sequence at times of human occupation.

Increasing terrestrial aridity and continentality over time, indicated by both proxy and modelled data (Figure 12 and Figure 13) is accompanied by evidence of increased cultural complexity, which is manifested in more diverse and sophisticated symbolic artefacts and tools produced from a diversity of raw materials (d'Errico et al., 2005; Henshilwood et al., 2001; Henshilwood et al. 2002; Henshilwood et al. 2004; Henshilwood and Dubreuil, 2011; Henshilwood et al., 2018; Soriano et al., 2007; Wadley, 2001). When the shoreline was close to BBC during periods of higher sea level, the climate was coastal with more humid conditions in the surrounding landscape and smaller interseasonal and diurnal ranges of temperatures (Figure 12 and Figure 13). Evidence suggests high shellfish consumption alongside small shrubland browsers and tortoises (Thompson and Henshilwood, 2014) - a rich and stable environment that potentially enabled high levels of self-sufficiency which may have limited interactions between groups and across large distances (Whallon, 2006; Ambrose, 2010). These conditions might have also reduced the need for mobility and favoured longer stays at BBC, as indicated by the site usage reconstruction by Haaland et al. (2020).

As the sea-level dropped and the shoreline moved further from the cave, continentality increased and resources may have become more unpredictable and scattered. A way hunter-gatherers would adapt to increasing aridity/continentality is by increasing their mobility radius (Whallon, 2006; Haaland et al., 2020). By doing so, paths with other populations would be crossed more often, hence people would interact more frequently. This increased interaction would enhance culture and knowledge exchange among people, which can in turn boost the development of skill levels ultimately portrayed in the archaeological record by increased material complexity (Grove, 2016). The BBC archaeological record implies that its occupants faced varying environmental conditions through the period of occupation (Figure 12), thus they adapted their subsistence patterns accordingly, as revealed by more frequent but shorter visits to the cave (Haaland et al., 2020). This is further accentuated by evidence of changes in foraging linked to less shell fishing and an increase in the exploitation of larger, more gregarious ungulates (Reynard and Henshilwood, 2018; 2019). An increase in the use of silcrete as raw material for tool making, particularly bifacial points in the later Still Bay layers, reflects the shifting mobility patterns as the environment changed (Henshilwood et al., 2001; Reynard and Henshilwood, 2017).

Higher mobility meant more frequent encounters with neighbouring groups, potentially giving rise to extended network social structures (McBrearty and Brooks, 2000), but also to more potential for conflicts. In order to reduce risk situations with other groups, historical hunter-gatherers practised long-distance contact and had exchange systems in place in order to help maintain stable population numbers (Mendoza Straffon, 2014). To sustain such networks among different groups over large distances, constant maintenance and reinforcement were required, usually through symbolic and ritual practices (Mendoza Straffon, 2014). Artifacts of a clearly symbolic nature such as ochre, and the use of marine shells in symbolic contexts may be testimonials of 'symbolically mediated behaviour' (Henshilwood and Marean, 2003).

## 5 Summary and conclusion

In this study we employed a targeted modelling approach to assess climatic changes in the vicinity of Blombos Cave (BBC) and the surrounding region of the southern Cape of South Africa from 82 to 70 ka. The results from the dynamical models (summarised in Figure 13) were compared with the  $\delta^2\text{H}$  values of leaf wax *n*-alkanes (Figure 12). These biomarkers provide observations of changing hydroclimate conditions and were derived directly from within the cave's stratigraphic sequence. As such, they present one of the first records of its kind produced in an archaeological setting in this area. Overall, both lines of evidence point towards drying of the region and the immediate vicinity of BBC at 70 ka as a result of weaker westerly winds in winter and cooler SSTs, as well as the expanding coastal plain and the resulting shift towards a more continental climate. Due to the coastline shift and increased land area at 70 ka, there are year-round reductions in rainfall. This is on top of the decline in winter precipitation arising from orbital forcing only (through weaker westerlies and a cooler Agulhas current at 70 ka). Both the diurnal and the inter-seasonal range of temperatures became significantly larger. Summer daytime temperatures are especially higher at 70 ka, contributing to the drying signal through enhanced evaporation. The climate simulations are consistent with observations of leaf wax *n*-alkane  $\delta^2\text{H}$  values that record an increase in  $\delta^2\text{H}$  of soil moisture, likely in response to increased evaporative fractionation under relatively more arid conditions. These findings are in broad agreement with previous studies but provide important new details and direct quantification of the changing climate characteristics, and further suggest that local features played a critical role in modifying the regional climate and environment.

Placing our findings in the context of previous studies on BBC, and proposed site use and subsistence patterns of the early human inhabitants of the cave; the changes in local climate from 82 to 70 ka, more likely than not, influenced human behaviour. The climate change patterns observed locally at BBC may imply similar and widespread changes in the southern Cape during MIS 5-4, though more work using high resolution modelling and cave site-based climate reconstruction is needed to evaluate this. Our study demonstrates the importance of representing local scales in paleoclimate modelling, as well as the benefits of integrating on-site proxy reconstructions, archaeological evidence and numerical approaches.

## Data availability statement

The raw data supporting the conclusion of this article will be made available by the authors, without undue reservation.

## Author contributions

ZZ designed and performed the global climate model simulations. OG and SS designed the regional climate model simulations and analyzed and interpreted the output. OG performed the regional climate model simulations and drafted together with MS the initial manuscript. MS designed the *n*-alkane study, acquired funding for fieldwork, sampling, and analysis of sediment, sampled the cave sediments, and interpreted the data. WV, PM, and WD'A. extracted, separated, and measured all analyzed biomarkers. All authors contributed to the article and approved the submitted version.

## Funding

Stable isotope analyses were done at the Norwegian National Infrastructure project FARLAB (Facility for advanced isotopic research and monitoring of weather, climate, and biogeochemical cycling, Project Nr. 245907) at the University of Bergen, Norway. MS, WV, and PM acknowledge funding for the pilot data study to carry out the analytical work on Blombos Cave through the Bjerknes Centre for Climate research (Norway) Fast-Track Initiatives scheme (CAVEWAX). Additional support was provided to WV by the Momentum program of the University of Bergen, and a Trond Mohn foundation (TMS) Starting Grant (TMS2021STG01). This work was partly supported by the Research Council of Norway, through its Centres of Excellence funding scheme, SFF Centre for Early Sapiens behaviour (SapienCE), project number 262618. The simulations in this study were performed on resources provided by Sigma2 - the National Infrastructure for High Performance Computing and Data Storage in Norway through projects: NN9486K and NS9486K. The open access publication was covered by University of

Bergen. Additional funding to CH came from a South African National Research Foundation Research Chair (SARChI) at the University of the Witwatersrand. The funders had no role in study design, data collection and analysis, decision to publish, or preparation of the manuscript.

## Acknowledgments

We thank Priscilla Mooney and Deniz Bozkurt for their technical support throughout WRF model set-up and simulations, John Galewsky for providing his modified WRF source code that implements the use of palaeo-orbital parameters, and Jimwoong Yoo for his explanations of the aforementioned code. We also thank colleagues from the SFF Centre for Early Sapiens Behaviour for useful and stimulating discussions.

## Conflict of interest

The authors declare that the research was conducted in the absence of any commercial or financial relationships that could be construed as a potential conflict of interest.

## Publisher's note

All claims expressed in this article are solely those of the authors and do not necessarily represent those of their affiliated organizations, or those of the publisher, the editors and the reviewers. Any product that may be evaluated in this article, or claim that may be made by its manufacturer, is not guaranteed or endorsed by the publisher.

## Supplementary material

The supplementary material for this article can be found online at: <https://www.frontiersin.org/articles/10.3389/feart.2023.1198068/full#supplementary-material>

## References

- Ambrose, S. H. (2010). Coevolution of composite-tool technology, constructive memory, and language: Implications for the evolution of modern human behavior. *Curr. Anthropol.* 51, S135–S147. doi:10.1086/650296
- Berger, A., and Loutre, M. F. (1991). Insolation values for the climate of the last 10 million years. *Quat. Sci. Rev.* 10, 297–317. doi:10.1016/0277-3791(91)90033-q
- Braun, K., Bar-Matthews, M., Ayalon, A., Zilberman, T., and Matthews, A. (2017). Rainfall isotopic variability at the intersection between winter and summer rainfall regimes in coastal South Africa (Mossel Bay, Western Cape Province). *South Afr. J. Geol.* 120, 323–340. doi:10.25131/gssajg.120.3.323
- Bray, E. E., and Evans, E. D. (1961). Distribution of n-paraffins as a clue to recognition of source beds. *Geochimica Cosmochimica Acta* 22, 2–15. doi:10.1016/0016-7037(61)90069-2
- Carr, A. S., Boom, A., Grimes, H. L., Chase, B. M., Meadows, M. E., and Harris, A. (2014). Leaf wax *n*-alkane distributions in arid zone South African flora: Environmental controls, chemotaxonomy and palaeoecological implications. *Org. Geochem.* 67, 72–84. doi:10.1016/j.orggeochem.2013.12.004
- Carr, A. S., Chase, B. M., and Mackay, A. (2016). "Mid to late quaternary landscape and environmental dynamics in the Middle stone age of southern South Africa," in *Africa from MIS 6-2: Population dynamics and palaeoenvironments*. Editors Jones, S. C., and Stewart, B. A. (Dordrecht: Springer Netherlands), 23–47.
- Cawthra, H. C., Jacobs, Z., Compton, J. S., Fisher, E. C., Karkanas, P., and Marean, C. W. (2018). Depositional and sea-level history from MIS 6 (Termination II) to MIS 3 on the southern continental shelf of South Africa. *Quat. Sci. Rev.* 181, 156–172. ISSN 0277-3791. doi:10.1016/j.quascirev.2017.12.002
- Cawthra, H. C., Anderson, R. J., De Vynck, J. C., Jacobs, Z., Jerardino, A., Kyriacou, K., et al. (2020). Migration of Pleistocene shorelines across the Palaeo-Agulhas Plain: Evidence from dated sub-bottom profiles and archaeological shellfish assemblages. *Quat. Sci. Rev.* 235, 106107. doi:10.1016/j.quascirev.2019.106107
- Collins, J. A., Carr, A. S., Schefuß, E., Boom, A., and Sealy, J. (2017). Investigation of organic matter and biomarkers from Diepkloof Rock shelter, south Africa: Insights into Middle stone age site usage and palaeoclimate. *J. Archaeol. Sci.* 85, 51–65. doi:10.1016/j.jas.2017.06.011
- Copeland, S. R., Cawthra, H. C., Fisher, E. C., Lee-Thorp, J. A., Cowling, R. M., le Roux, P. J., et al. (2016). Strontium isotope investigation of ungulate movement patterns on the pleistocene paleo-agulhas plain of the greater Cape floristic region, south Africa. *Quat. Sci. Rev.* 141, 65–84. doi:10.1016/j.quascirev.2016.04.002
- Dansgaard, W. (1964). Stable isotopes in precipitation. *Tellus* 16, 436–468. doi:10.3402/tellusa.v16i4.8993
- d'Errico, F., and Henshilwood, C. S. (2007). Additional evidence for bone technology in the southern african Middle stone age. *J. Hum. Evol.* 52, 142–163. doi:10.1016/j.jhevol.2006.08.003

- Dorale, J. A., Onac, B. P., Fornós, J. J., Ginés, J., Ginés, A., Tuccimei, P., et al. (2010). Sea-level highstand 81,000 years ago in Mallorca. *Science* 327 (5967), 860–863. doi:10.1126/science.1181725
- Duplessy, J.-C., Labeyrie, L., and Waelbroeck, C. (2002). Constraints on the ocean oxygen isotopic enrichment between the last glacial maximum and the holocene: Paleoclimatological implications. *Quat. Sci. Rev.* 21 (1–3), 315–330. doi:10.1016/S0277-3791(01)00107-X
- Eglinton, G., and Hamilton, R. J. (1967). Leaf epicuticular waxes. *Science* 156, 1322–1335. doi:10.1126/science.156.3780.1322
- Engelbrecht, C. J., and Landman, W. A. (2016). Interannual variability of seasonal rainfall over the Cape south coast of South Africa and synoptic type association. *Clim. Dyn.* 47, 295–313. doi:10.1007/s00382-015-2836-2
- Fick, S. E., and Hijmans, R. J. (2017). WorldClim 2: New 1-km spatial resolution climate surfaces for global land areas. *Int. J. Climatol.* 37, 4302–4315. doi:10.1002/joc.5086
- Göktürk, O. M., Sobolowski, S. P., Simon, M. H., Zhang, Z., and Jansen, E. (2023). Sensitivity of coastal southern African climate to changes in coastline position and associated land extent over the last glacial. *Quat. Sci. Rev.* 300, 107893. doi:10.1016/j.quascirev.2022.107893
- Goldberg, P., Miller, C. E., Schiegl, S., Ligouis, B., Berna, F., Conard, N. J., et al. (2009). Bedding, hearths, and site maintenance in the Middle stone age of Sibudu cave, KwaZulu-natal, south Africa. *Archaeol. Anthropol. Sci.* 1, 95–122. doi:10.1007/s12520-009-0008-1
- Gonfiantini, R., Roche, M.-A., Olivry, J.-C., Fontes, J.-C., and Zuppi, G. M. (2001). The altitude effect on the isotopic composition of tropical rains. *Chem. Geol.* 181, 147–167. doi:10.1016/S0009-2541(01)00279-0
- Grant, K. M., Rohling, E. J., Bar-Matthews, M., Ayalon, A., Medina-Elizalde, M., Ramsey, C. B., et al. (2012). Rapid coupling between ice volume and polar temperature over the past 150,000 years. *Nature* 491, 744–747. doi:10.1038/nature11593
- Grove, M. (2016). Population density, mobility, and cultural transmission. *J. Archaeol. Sci.* 74, 75–84. doi:10.1016/j.jas.2016.09.002
- Guo, C., Bentsen, M., Bethke, I., Ilicak, M., Tjiputra, J., Toniazzo, T., et al. (2019). Description and evaluation of NorESM1-F: A fast version of the Norwegian earth system model (NorESM). *Geosci. Model. Dev.* 12, 343–362. doi:10.5194/gmd-12-343-2019
- Haaland, M. M., Miller, C. E., Unhammer, O. F., Reynard, J. P., van Niekerk, K. L., Ligouis, B., et al. (2020). Geoaerchaeological investigation of occupation deposits in Blombos Cave in South Africa indicate changes in site use and settlement dynamics in the southern Cape during MIS 5b-4. *Quat. Res.* 100, 170–223. doi:10.1017/qua.2020.75
- Harris, C., Burgers, C., Miller, J., and Rawoot, F. (2010). O-and H-isotope record of Cape Town rainfall from 1996 to 2008, and its application to recharge studies of table mountain groundwater, South Africa. *South Afr. J. Geol.* 113, 33–56. doi:10.2113/gssajg.113.1.33
- Haywood, A. M., Dowsett, H. J., Otto-Bliesner, B., Chandler, M. A., Dolan, A. M., Hill, D. J., et al. (2010). Pliocene model intercomparison project (PlioMIP): Experimental design and boundary conditions (experiment 1). *Model. Dev.* 3, 227–242. doi:10.5194/gmd-3-227-2010
- Henshilwood, C., d'Errico, F., Vanhaeren, M., Van Niekerk, K., and Jacobs, Z. (2004). Middle stone age shell beads from South Africa. *Science* 304, 404. doi:10.1126/science.1095905
- Henshilwood, C. S., and Dubreuil, B. (2011). The Still Bay and Howiesons Poort, 77–59 ka: Symbolic material culture and the evolution of the mind during the african Middle stone age. *Curr. Anthropol.* 52, 361–400. doi:10.1086/660022
- Henshilwood, C. S., and Marean, C. W. (2003). The origin of modern human behavior: Critique of the models and their test implications. *Curr. Anthropol.* 44, 627–651. doi:10.1086/377665
- Henshilwood, C. S., d'Errico, F., Marean, C. W., Milo, R. G., and Yates, R. (2001). An early bone tool industry from the Middle stone age at Blombos cave, South Africa: Implications for the origins of modern human behaviour, symbolism and language. *J. Hum. Evol.* 41, 631–678. doi:10.1006/jhev.2001.0515
- Henshilwood, C. S., d'Errico, F., Yates, R., Jacobs, Z., Tribolo, C., Duller, G. A. T., et al. (2002). Emergence of modern human behavior: Middle stone age engravings from south Africa. *Science* 295, 1278–1280. doi:10.1126/science.1067575
- Henshilwood, C. S., d'Errico, F., van Niekerk, K. L., Coquinot, Y., Jacobs, Z., Lauritzen, S.-E., et al. (2011). A 100,000-year-old ochre-processing workshop at Blombos cave, south Africa. *Science* 334, 219–222. doi:10.1126/science.1211535
- Henshilwood, C. S., van Niekerk, K. L., Wurz, S., Delagnes, A., Armitage, S. J., Rifkin, R. F., et al. (2014). Klipdrift shelter, southern Cape, South Africa: Preliminary report on the Howiesons Poort layers. *J. Archaeol. Sci.* 45, 284–303. doi:10.1016/j.jas.2014.01.033
- Henshilwood, C. S., d'Errico, F., van Niekerk, K. L., Dayet, L., Queffelec, A., and Pollarolo, L. (2018). An abstract drawing from the 73,000-year-old levels at Blombos Cave, South Africa. *Nature* 562, 115–118. doi:10.1038/s41586-018-0514-3
- Henshilwood, C. S. (2012). Late pleistocene techno-traditions in southern Africa: A review of the Still Bay and Howiesons Poort, c 75–59 ka. *J. World Prehistory* 25, 205–237. doi:10.1007/s10963-012-9060-3
- Herrera-Herrera, A. V., Leierer, L., Jambrina-Enríquez, M., Connolly, R., and Mallol, C. (2020). Evaluating different methods for calculating the Carbon Preference Index (CPI): Implications for palaeoecological and archaeological research. *Org. Geochem.* 146, 104056. doi:10.1016/j.orggeochem.2020.104056
- Herrmann, N., Boom, A., Carr, A. S., Chase, B. M., Granger, R., Hahn, A., et al. (2016). Sources, transport and deposition of terrestrial organic material: A case study from southwestern Africa. *Quat. Sci. Rev.* 149, 215–229. doi:10.1016/j.quascirev.2016.07.028
- Herrmann, N., Boom, A., Carr, A. S., Chase, B. M., West, A. G., Zabel, M., et al. (2017). Hydrogen isotope fractionation of leaf wax *n*-alkanes in southern African soils. *Org. Geochem.* 109, 1–13. doi:10.1016/j.orggeochem.2017.03.008
- Hersbach, H., Bell, B., Berrisford, P., Hirahara, S., Horányi, A., Muñoz-Sabater, J., et al. (2020). The ERA5 global reanalysis. *Q. J. R. Meteorol. Soc.* 146, 1999–2049. doi:10.1002/qj.3803
- Jacobs, Z., Jones, B. G., Cawthra, H. C., Henshilwood, C. S., and Roberts, R. G. (2020). The chronological, sedimentary and environmental context for the archaeological deposits at Blombos Cave, South Africa. *Quat. Sci. Rev.* 235, 105850. doi:10.1016/j.quascirev.2019.07.032
- Langejans, G. H. J., van Niekerk, K. L., Dusseldorp, G. L., and Thackeray, J. F. (2012). Middle stone age shellfish exploitation: Potential indications for mass collecting and resource intensification at Blombos cave and Klasies River, south Africa. *Quat. Int.* 270, 80–94. doi:10.1016/j.quaint.2011.09.003
- Levitus, S., and Boyer, T. P. (1994). *World Ocean atlas volume 4: Temperature*. Washington, DC: NOAA Atlas NESDIS 4, US Government Printing Office, 117.
- Lombard, M. (2011). Quartz-tipped arrows older than 60 ka: Further use-trace evidence from Sibudu, KwaZulu-natal, south Africa. *J. Archaeol. Sci.* 38, 1918–1930. doi:10.1016/j.jas.2011.04.001
- Marean, C. W., Bar-Matthews, M., Bernatchez, J., Fisher, E., Goldberg, P., Herries, A. I. R., et al. (2007). Early human use of marine resources and pigment in South Africa during the Middle Pleistocene. *Nature* 449, 905–908. doi:10.1038/nature06204
- Marean, C. W., Bar-Matthews, M., Fisher, E., Goldberg, P., Herries, A., Karkanas, P., et al. (2010). The stratigraphy of the Middle stone age sediments at Pinnacle point cave 13B (mossel Bay, western Cape province, South Africa). *J. Hum. Evol.* 59, 234–255. doi:10.1016/j.jhevol.2010.07.007
- Marean, C. W., Cawthra, H. C., Cowling, R. M., Esler, K. J., Fisher, E., Milewski, A., et al. (2014). “Stone age people in a changing South African greater Cape floristic region,” in *Fynbos: Ecology, evolution, and conservation of a megadiverse region*. Editors N. Allsopp, J. F. Colville, and G. A. Verboom (Oxford University Press), 0.
- Marean, C. W., Cowling, R. M., and Franklin, J. (2020). The Palaeo-Agulhas Plain: Temporal and spatial variation in an extraordinary extinct ecosystem of the pleistocene of the Cape floristic region. *Quat. Sci. Rev.* 235, 106161. doi:10.1016/j.quascirev.2019.106161
- Marean, C. W. (2014). The origins and significance of coastal resource use in Africa and Western Eurasia. *J. Hum. Evol.* 77, 17–40. doi:10.1016/j.jhevol.2014.02.025
- Martínez-Botí, M., Foster, G., Chalk, T., Rohling, E. J., Sexton, P. F., Lunt, D. J., et al. (2015). Plio-Pleistocene climate sensitivity evaluated using high-resolution CO<sub>2</sub> records. *Nature* 518, 49–54. doi:10.1038/nature14145
- McBrearty, S., and Brooks, A. S. (2000). The revolution that wasn't: A new interpretation of the origin of modern human behavior. *J. Hum. Evol.* 39, 453–563. doi:10.1006/jhev.2000.0435
- Mendoza Straffon, L. (2014). *Art in the making: The evolutionary origins of visual art as a communication signal/larissa mendoza Straffon*. Dissertation Leiden University in order to obtain the degree of doctor in the year 2014. Available at: <https://scholarlypublications.universiteitleiden.nl/handle/1887/28698>.
- Mourre, V., Villa, P., and Henshilwood, C. S. (2010). Early use of pressure flaking on lithic artifacts at Blombos cave, south Africa. *Science* 330, 659–662. doi:10.1126/science.1195550
- Mucina, L., and Rutherford, M. C. (2006). *The Vegetation of South Africa, Lesotho and Swaziland*. Strelitzia 19. Pretoria: South African National Biodiversity Institute.
- Nel, T. H., and Henshilwood, C. S. (2016). The small mammal sequence from the c 76 – 72 ka Still Bay levels at Blombos cave, South Africa – taphonomic and palaeoecological implications for human behaviour. *PLOS ONE* 11, e0159817. doi:10.1371/journal.pone.0159817
- Nel, T. H., and Henshilwood, C. S. (2021). The 100,000–77,000-year old Middle stone age micromammal sequence from Blombos cave, south Africa: Local climatic stability or a tale of predator bias? *Afr. Archaeol. Rev.* 38, 443–476. doi:10.1007/s10437-021-09444-8
- Nicholson, S. E. (2000). The nature of rainfall variability over Africa on time scales of decades to millennia. *Glob. Planet. Change* 26, 137–158. doi:10.1016/S0921-8181(00)00040-0
- Pico, T., Creveling, J. R., and Mitrovica, J. X. (2017). Sea-Level records from the U.S. Mid-atlantic constrain laurentide ice sheet extent during marine isotope stage 3. *Nat. Commun.* 8, 15612. doi:10.1038/ncomms15612
- Porraz, G., Parkington, J. E., Schmidt, P., Bereziat, G., Brugal, J.-P., Dayet, L., et al. (2021). Experimentation preceding innovation in a MIS5 Pre-Still Bay layer from

- Diepkloof Rock Shelter (South Africa): emerging technologies and symbols. *Peer Community J.* 1. doi:10.24072/pcjournal.27
- Powers, J. G., Klemp, J. B., Skamarock, W. C., Davis, C. A., Dudhia, J., Gill, D. O., et al. (2017). The weather research and forecasting model: Overview, system efforts, and future directions. *Bull. Am. Meteorological Soc.* 98 (8), 1717–1737. doi:10.1175/bams-d-15-00308.1
- Poynter, J. G., Farrimond, P., Robinson, N., and Eglinton, G. (1989). “Aeolian-derived higher plant lipids in the marine sedimentary record: Links with palaeoclimate,” in *Palaeoclimatology and palaeometeorology: Modern and past patterns of global atmospheric transport*. Editors Leinen, M., and Sarntheim, M. (Dordrecht: Springer Netherlands), 435–462.
- Reynard, J. P., and Henshilwood, C. S. (2017). Subsistence strategies during the late pleistocene in the southern Cape of South Africa: Comparing the Still Bay of Blombos cave with the Howiesons Poort of Klipdrift shelter. *J. Hum. Evol.* 108, 110–130. doi:10.1016/j.jhevol.2017.04.003
- Reynard, J. P., and Henshilwood, C. S. (2018). Using trampling modification to infer occupational intensity during the Still Bay at Blombos cave, southern Cape, south Africa. *Afr. Archaeol. Rev.* 35, 1–19. doi:10.1007/s10437-018-9286-2
- Reynard, J. P., and Henshilwood, C. S. (2019). Environment versus behaviour: Zooarchaeological and taphonomic analyses of fauna from the Still Bay layers at Blombos cave, south Africa. *Quat. Int.* 500, 159–171. doi:10.1016/j.quaint.2018.10.040
- Roberts, P., Henshilwood, C. S., van Niekerk, K. L., Keene, P., Gledhill, A., Reynard, J., et al. (2016). Climate, environment and early human innovation: Stable isotope and faunal proxy evidence from archaeological sites (98–59ka) in the southern Cape, south Africa. *PLOS ONE* 11, e0157408. doi:10.1371/journal.pone.0157408
- Rohling, E. J., Foster, G. L., Grant, K. M., Marino, G., Roberts, A. P., Tamisiea, M. E., et al. (2014). Sea-level and deep-sea-temperature variability over the past 5.3 million years. *Nature* 508, 477–482. doi:10.1038/nature13230
- Sachse, D., Billault, I., Bowen, G. J., Chikaraishi, Y., Dawson, T. E., Feakins, S. J., et al. (2012). Molecular paleohydrology: Interpreting the hydrogen-isotopic composition of lipid biomarkers from photosynthesizing organisms. *Annu. Rev. Earth Planet. Sci.* 40, 221–249. doi:10.1146/annurev-earth-042711-105535
- Schefuß, E., Ratmeyer, V., Stuut, J.-B. W., Jansen, J. H. F., and Sinninghe Damsté, J. S. (2003). Carbon isotope analyses of *n*-alkanes in dust from the lower atmosphere over the central eastern Atlantic. *Geochimica Cosmochimica Acta* 67, 1757–1767. doi:10.1016/s0016-7037(02)01414-x
- Schefuß, E., Schouten, S., and Schneider, R. R. (2005). Climatic controls on central African hydrology during the past 20,000 years. *Nature* 437, 1003–1006. doi:10.1038/nature03945
- Singarayer, J. S., and Burrough, S. L. (2015). Interhemispheric dynamics of the African rainbelt during the late Quaternary. *Quat. Sci. Rev.* 124, 48–67. doi:10.1016/j.quascirev.2015.06.021
- Skamarock, W. C., Klemp, J. B., Dudhia, J., Gill, D. O., Liu, Z., Berner, J., et al. (2019). *A description of the advanced research WRF model version 4 (No. NCAR/TN-556+STR)*. doi:10.5065/1dfh-6p97
- Soriano, S., Villa, P., and Wadley, L. (2007). Blade technology and tool forms in the Middle stone age of SouthSouth Africa: The Howiesons Poort and post-Howiesons Poort at rose cottage cave. *J. Archaeol. Sci.* 34, 681–703. doi:10.1016/j.jas.2006.06.017
- Soriano, S., Villa, P., Delagnes, A., Degano, I., Pollarolo, L., Lucejko, J. J., et al. (2015). The Still Bay and Howiesons Poort at sibudu and Blombos: Understanding Middle stone age technologies. *PLOS ONE* 10, e0131127. doi:10.1371/journal.pone.0131127
- Spratt, R. M., and Lisiecki, L. E. (2016). A Late Pleistocene sea level stack. *Clim. Past* 12, 1079–1092. doi:10.5194/cp-12-1079-2016
- Strobel, P., Haberzettl, T., Bliedtner, M., Struck, J., Glaser, B., Zech, M., et al. (2020). The potential of  $\delta^2\text{H}$  *n*-alkanes and  $\delta^{18}\text{O}$  sugar for palaeoclimate reconstruction – a regional calibration study for South Africa. *Sci. Total Environ.* 716, 137045. doi:10.1016/j.scitotenv.2020.137045
- Strobel, P., Bliedtner, M., Carr, A. S., Struck, J., du Plessis, N., Glaser, B., et al. (2022). Reconstructing late quaternary precipitation and its source on the southern Cape coast of SouthSouth Africa: A multi-proxy paleoenvironmental record from Vankervelsvlei. *Quat. Sci. Rev.* 284, 107467. doi:10.1016/j.quascirev.2022.107467
- Texier, P.-J., Porraz, G., E., Parkington, J., Rigaud, J.-P., Poggenpoel, C., and Tribolo, C. (2013). The context, form and significance of the MSA engraved ostrich eggshell collection from Diepkloof Rock Shelter, Western Cape, South Africa. *J. Archaeol. Sci.* 40, 3412–3431. doi:10.1016/j.jas.2013.02.021
- Thompson, J., and Henshilwood, C. S. (2014). Nutritional values of tortoises relative to ungulates from the Middle Stone Age levels at Blombos Cave, South Africa: Implications for foraging and social behaviour. *J. Hum. Evol.* 67, 33–47. doi:10.1016/j.jhevol.2013.09.010
- Thompson, L. G., Davis, M. E., Mosley-Thompson, E., Lin, P.-N., Henderson, K. A., and Mashiotta, T. A. (2005). Tropical ice core records: evidence for asynchronous glacial on Milankovitch timescales. *J. Quaternary Sci.* 20, 723–733.
- Tribolo, C., Mercier, N., Douville, E., Joron, J. L., Reyss, J. L., Rufer, D., et al. (2013). OSL and TL dating of the Middle stone age sequence at Diepkloof Rock shelter (South Africa): A clarification. *J. Archaeol. Sci.* 40, 3401–3411. doi:10.1016/j.jas.2012.12.001
- Vahdati, A. R., Weissmann, J. D., Timmermann, A., Ponce de León, M. S., and Zollikofer, C. P. E. (2019). Drivers of late pleistocene human survival and dispersal: An agent-based modeling and machine learning approach. *Quat. Sci. Rev.* 221, 105867. doi:10.1016/j.quascirev.2019.105867
- Venter, J. A., Brooke, C. F., Marean, C. W., Fritz, H., and Helm, C. W. (2020). Large mammals of the Palaeo-Agulhas Plain showed resilience to extreme climate change but vulnerability to modern human impacts. *Quat. Sci. Rev.* 235, 106050. doi:10.1016/j.quascirev.2019.106050
- Wadley, L., Esteban, L., de la Peña, P., Wojcieszak, M., Stratford, D., Lennox, S., et al. (2020). Fire and grass-bedding construction 200 thousand years ago at Border Cave, South Africa. *Science* 369, 863–866. doi:10.1126/science.abc7239
- Wadley, L. (2001). What is cultural modernity? A general view and a South African perspective from rose cottage cave. *Camb. Archaeol. J.* 11, 201–221. doi:10.1017/s0959774301000117
- Weldon, D., and Reason, C. J. C. (2014). Variability of rainfall characteristics over the South coast region of South Africa. *Theor. Appl. Climatol.* 115, 177–185. doi:10.1007/s00704-013-0882-4
- Whallon, R. (2006). Social networks and information: Non-“utilitarian” mobility among hunter-gatherers. *J. Anthropol. Archaeol.* 25, 259–270. doi:10.1016/j.jaa.2005.11.004
- Wiesenberg, G. L. B., Lehdorff, E., and Schwark, L. (2009). Thermal degradation of rye and maize straw: Lipid pattern changes as a function of temperature. *Org. Geochem.* 40, 167–174. doi:10.1016/j.orggeochem.2008.11.004
- Will, M., Conard, N., and Tryon, C. (2019). *Timing and trajectory of cultural evolution on the African continent 200,000-30,000 years ago*, 25–72.
- Windler, G., Tierney, J. E., Zhu, J., and Poulsen, C. J. (2020). Unraveling glacial hydroclimate in the indo-pacific warm pool: Perspectives from water isotopes. *Paleoceanogr. Paleoclimatology* 35, e2020PA003985. doi:10.1029/2020pa003985
- Wurz, S. (2002). Variability in the Middle stone age lithic sequence, 115,000–60,000 Years ago at Klasies River, south Africa. *J. Archaeol. Sci.* 29, 1001–1015. doi:10.1006/jasc.2001.0799
- Yesner, D. R., Ayres, W. S., Carlson, D. L., Davis, R. S., Dewar, R., Manuel, R. G., et al. (1980). Maritime hunter-gatherers: Ecology and prehistory [and comments and reply]. *Curr. Anthropol.* 21, 727–750. doi:10.1086/202568
- Yoo, J., Galewsky, J., Camargo, S. J., Korty, R., and Zamora, R. (2016). Dynamical downscaling of tropical cyclones from CCSM4 simulations of the Last Glacial Maximum. *J. Adv. Model. Earth Syst.* 8, 1229–1247. doi:10.1002/2016ms000685
- Zhang, Z., and Yan, Q. (2012). Pre-industrial and mid-pliocene simulations with NorESM-L: AGCM simulations. *Geosci. Model. Dev.* 5, 1033–1043. doi:10.5194/gmd-5-1033-2012